Environmental Modelling and Software 204 (2026) 107056

Contents lists available at ScienceDirect

Environmental Modelling and Software

journal homepage: www.elsevier.com/locate/envsoft

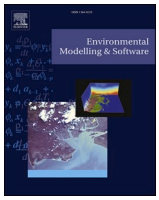

Modelling the human impact on hydrological cycle: The *MISDc v3.1* model

Sindhu Kalimisetty [a], Alberto Montanari [b], Serena Ceola [b], Irene Palazzoli [b], Paolo Stocchi [c], Paolo Filippucci [a], Luca Brocca [a], Jacopo Dari [a,d], Francesco Tornatore [e], Federica Bonaiuti [e], Stefania Camici [a,*]

[a] National Research Council, Research Institute for Geo-Hydrological Protection, Perugia, Italy
[b] Department of Civil, Chemical, Environmental, and Materials Engineering, Alma Mater Studiorum Università di Bologna, Bologna, Italy
[c] Institute of Atmospheric Sciences and Climate, National Research Council (CNR-ISAC), Bologna, 40129, Italy
[d] Department of Civil and Environmental Engineering, University of Perugia, Perugia, Italy
[e] Po River Basin District Authority (ADBPO), Parma, Italy

ARTICLE INFO

Keywords:
Satellite products
Soil moisture
Conceptual hydrological modelling
Irrigation
Water uses
Drought
Po basin

ABSTRACT

This study presents *MISDc v3.1*, a process-based, flexible and open-source hydrological model developed to simulate complex water dynamics in large and human-impacted river systems. The model is applied to the Po River basin, Italy, subjected to strong anthropogenic impact. Calibration uses hydrometeorological data from 2000 to 2023, while validation is performed through multi-variable comparison against observed river discharge and satellite-based measurements of soil moisture, evaporation, snow water equivalent, and irrigation volumes. Quantitative performance assessment indicates strong simulation accuracy across multiple gauge stations (modified Kling–Gupta Efficiency = 0.88–0.93). The inclusion of irrigation and reservoir operation modules markedly enhances river discharge simulations, particularly during low-flow conditions and the 2022–2023 extreme drought. Uncertainty, assessed through the BLUECAT method, fosters a better understanding of model reliability across flow regimes. Owing to its Python-based and open-access architecture, *MISDc v3.1* is easily transferable to other basins, offering a robust and flexible tool for integrated water resources management.

1. Introduction

Mathematical modelling of catchment hydrology has evolved from simple empirical approaches to sophisticated distributed models able to integrate GIS capabilities, advanced computational methods as well as remote sensing data to address complex environmental and water resources challenges (Singh, 2018). Despite these advances, predicting extreme hydrological events in human-altered river basins remains particularly challenging due to the intertwined effects of climate variability, land-use change and anthropogenic activities (such as irrigation and reservoir regulation), which substantially modify natural hydrological processes. Hydrological droughts, in particular, emerge from the combined influence of climatic forcing and human activities, requiring modelling frameworks that explicitly represent both natural and anthropogenic factors (AghaKouchak et al., 2021; Rivera et al., 2021).

Several studies have demonstrated that human water demands strongly affect hydrological dynamics, especially during low-flow conditions (Liu et al., 2017). Explicit representation of irrigation processes has been shown to significantly improve low-flow and streamflow simulations (Droppers et al., 2020; Alfieri et al., 2021; Montanari et al., 2023; Wang et al., 2023; Zhang et al., 2023; Avanzi et al., 2024; De Lannoy et al., 2024; Bruno et al., 2024). For example, De Lannoy et al. (2024) reported a 12% improvement in reproducing summer streamflow during low-flow periods when irrigation modelling was included, while Rameshwaran et al. (2022) found a 10.7% improvement in low-flow simulation after accounting for irrigation abstractions in the Grid-to-Grid (G2G) model. Similarly, Bruno et al. (2024) highlighted a marked degradation in model performance during severe droughts when irrigation was neglected, identifying this omission as a primary cause of poor low-flow simulation.

Beyond irrigation, reservoir operations play a critical role in shaping both drought and flood dynamics. Reservoir water supply can mitigate short-term drought impacts by redistributing water seasonally (Wada et al., 2017) while inadequate representation of dams and reservoir operation rules can lead to unreliable flood simulations in regulated river systems (Wada et al., 2017; Veldkamp et al., 2018; Zhao et al.,

* Corresponding author. Research Institute for Geo-Hydrological Protection, National Research Council, Via della Madonna Alta 126, 06128, Perugia, Italy.
E-mail address: stefania.camici@cnr.it (S. Camici).

https://doi.org/10.1016/j.envsoft.2026.107056
Received 31 October 2025; Received in revised form 21 April 2026; Accepted 31 May 2026
Available online 6 June 2026

2020). In addition, other anthropogenic water uses such as domestic and industrial withdrawals can further modify river flow regimes. Although these abstractions are often smaller in magnitude compared to irrigation at the basin scale, their temporal persistence and spatial concentration near urban or industrial areas can substantially exacerbate hydrological deficits during droughts (Wada et al., 2013).

Together, these findings underscore the imperative for time-varying human impacts, such as water abstractions and reservoir operations by dams, to be integrated into hydrological models. Recent advances in large-scale hydrological modelling have increasingly focused on representing complex process interactions and time-varying human influences (see e.g., Burek et al., 2020; Telteu et al., 2021). While such developments enhance process realism, they often result in highly parameterized model structures and substantial computational demands. Importantly, increasing model complexity does not necessarily lead to improved predictive performance (see e.g. Li et al., 2015; Orth et al., 2015; Merz et al., 2022), but instead may exacerbate parameter non-identifiability and equifinality (Beven, 2006; Beven and Binley, 2014), particularly when observational data are limited. By contrast, more parsimonious conceptual hydrological models typically exhibit much lower computational costs and a limited number of calibration parameters, but often lack an explicit representation of anthropogenic influences and human–water interactions (Astagneau et al., 2021). These challenges highlight the need for parsimonious, modular hydrological modelling approaches that balance human-natural process representation, computational efficiency, and parameter identifiability (Beven and Chappell, 2021; Galelli et al., 2025).

In response to these challenges, this study presents the *MISDc v3.1* (semi-Distributed Continuous hydrologIcal Model) model, a parsimonious semi-distributed continuous rainfall–runoff model that explicitly integrates key anthropogenic water-use processes including irrigation, reservoir operations, and civil and industrial demands within a consistent hydrological framework. By representing the full water cycle while maintaining low computational complexity and a limited number of calibrated parameters, *MISDc v3.1* bridges the gap between conceptual and more complex models and is particularly suited for simulating extreme hydrological conditions, such as droughts, in catchments strongly influenced by human activities.

The *MISDc* model was firstly developed by Brocca et al. (2011, 2013) including soil and routing modules for the simulation of river discharge in natural basins. Subsequent developments by Massari et al. (2018) and Cislaghi et al. (2020) further improved the model structure, and numerous studies have demonstrated its robust ability to reproduce flood events across natural and near-natural basins under a wide range of climatic conditions (Masseroni et al., 2017; Camici et al., 2014, 2018, 2020; De Santis et al., 2021; Ding et al., 2022; Tramblay et al., 2023; Brocca et al., 2020, 2024). In particular, Cislaghi et al. (2020) conducted a comprehensive evaluation of the *MISDc* model over 63 mountainous catchments in the western Po Valley in Italy, demonstrating the robust performance of the model in simulating the high flows. However, both the original and the modified versions of the *MISDc* model (Brocca et al., 2011, 2013; Massari et al., 2018; Cislaghi et al., 2020) showed clear limitations in representing the hydrological cycle during drought periods in anthropized basins. More recently, Camici et al. (2025) adapted *MISDc* for water-resources management applications in the Po River basin; nevertheless, reservoir operations were not explicitly simulated, and water-use and irrigation components were tailored to a specific case study, limiting broader applicability. To address all these constraints, the *MISDc* model (v3.1) has been further refined in this study to represent both natural hydrological processes and anthropogenic activities affecting the water cycle, with the aim of improving the simulation of extreme hydrological events, particularly human-influenced droughts in highly managed river basins.

The model is evaluated over the Po river basin, one of Europe's most economically important and highly anthropized regions, supporting more than 18 million inhabitants, intensive agricultural production, and extensive industrial activities (Carminati and Martinelli, 2002; Musolino et al., 2017). The coexistence of multiple competing water uses, complex management infrastructures, and strong human regulation of river flows makes the basin a paradigmatic example of a human-modified hydrological system and a suitable testbed for *MISDc v3.1*. In recent decades, the basin has experienced recurrent hydrological extremes, including severe floods (e.g., October 2000; Castellarin et al., 2011) and prolonged droughts (e.g., the 2022 event; Montanari et al., 2023), whose frequency and intensity are expected to increase under climate change (Milly et al., 2008; Mazzoglio et al., 2025). These characteristics, common to many human-modified river basins worldwide, highlight the broader need for hydrological models that explicitly represent anthropogenic processes alongside natural dynamics in order to realistically simulate both flood and drought extremes.

The following sections introduce *MISDc v3.1* and demonstrate its capability to reproduce extreme hydrological conditions and drought dynamics in a highly managed basin. Coupled with a BLUECAT tool to assess its uncertainty, it provides river discharge estimates with confidence bounds as well as estimates of snow water equivalent, evaporation, superficial and root zone soil moisture and irrigation demands.

2. MISDc v3.1 modular hydrological model

The *MISDc v3.1* model is a flexible, modular, semi-distributed conceptual hydrological model able to reproduce the temporal evolution of the primary hydrological variables that regulate the water cycle both in near-natural and anthropized basins. To take into account the uncertainty in the river discharge simulations, the BLUECAT tool is used. It is able to transform a single deterministic model output into a probabilistic prediction providing additional insight into model reliability across varying flow regimes. The model code developed in Python, is freely available at https://github.com/sindhu-kalimisetty/MISDc-v3.1-Hydrological-Model and graphically illustrated in Fig. 1.

2.1. MISDc v3.1: model structure

The model includes an irrigation module (I_m), a reservoir module (Res_m), and a water use module ($CIWU_m$) to simulate the influence of anthropogenic activities on water resources, as well as a snow module (SN_m), a soil module (S_m), and a routing module (R_m) to represent the natural variability of water resources in response to climate forcing (see Fig. 1). All modules, except for routing and reservoir, can operate at the pixel scale when gridded input datasets are available. In contrast, routing uses basin-averaged runoff time series and is applied at the basin scale, while the reservoir module relies on the river discharge entering the dam. Concerning the temporal scale, all modules can operate from hourly to daily temporal scale, depending on the temporal resolution of the input data.

The following sections provide detailed descriptions of each module, except for the snow and routing modules, which are briefly summarized here; full details can be found in Camici et al. (2025). To ensure generality in the model description, it is assumed hereinafter that the input datasets are gridded denoting with N the number of sub-basins, N_C the number of pixels in each sub-basin, J_{irr} the number of the irrigated pixels in each sub-basin ($J_{irr} \in N_C$) and R the number of reservoirs. Each process pertaining to snow, soil and water use is repeated for each j^{th} pixel in the N^{th} sub-basin, with $j = \{1, \dots Nc\}$. Similarly, the irrigation module is applied to all J_{irr} irrigated pixels while the routing and reservoir modules are repeated N and R times, respectively (see Fig. 1). Conversely, if the input data are not gridded and only 1 time series is available for each basin, N_C is equal to *1*. It is hereby specified that henceforth, the description of each process will be made without the use of indexes, on the assumption that they are implied. Furthermore, depending on the temporal resolution of the input data (hourly or daily), the variables introduced below may be expressed in mm/h or mm/d. For the sake of generality, units are hereafter denoted as mm/t.

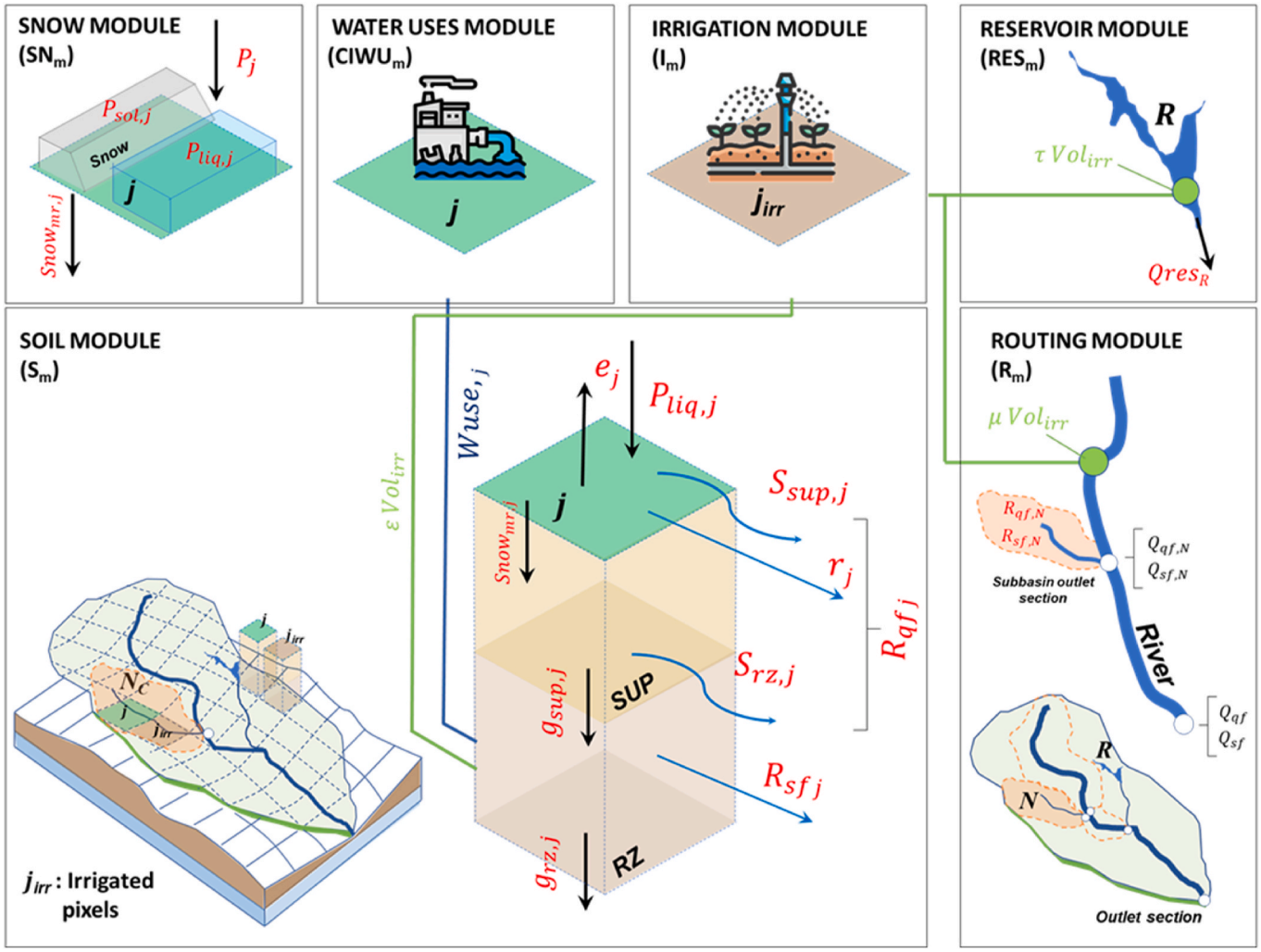

Fig. 1. Configuration of the *MISDc v3.1* model. The different panels illustrate the modules and their interconnections for modelling the hydrological cycle. Where N is the number of sub-basins, N_C is the number of pixels in each sub-basin, J_{irr} is the number of the irrigated pixels in each sub-basin, R represents number of reservoirs, P_j is the total precipitation for each j^{th} pixel, $P_{liq,j}$ and $P_{sol,j}$ is the precipitation separated into liquid and solid, $Snow_{mr,j}$ is the snow melt rate, e_j is the evaporation, r_j is the surface runoff, $S_{sup,j}$ and, $S_{rz,j}$ is the saturation excess from superficial and root zone soil layer, $R_{qf,j}$ and $R_{sf,j}$ is the quick-flow and slow-flow runoff responses, $g_{sup,j}$ is the percolation between soil layers, $g_{rz,j}$ is the deep percolation, $W_{use,j}$ is the percolation, $W_{use,j}$ is the water abstracted for civil and industrial activities, $Vol_{irr,j}$ is the total irrigation volume, τ ε, and μ, are coefficients indicating the portion of Vol_{irr} extracted from superficial water, root-zone soil layer, and reservoirs, $Qres_R$ is the reservoir outflow, $Q_{qf,N}$ and $Q_{sf,N}$ are the quick-flow and slow-flow river discharge components, SN_m is the snow module, S_m is the soil module, $CIWU_m$ is the civil and industrial water uses module, I_m is the irrigation module, Res_m is the reservoir module, R_m is the routing module.

2.1.1. Snow module (SN_m)

The snow module adopts a temperature-index (degree-day, Martinec, 1960) approach to partition precipitation and simulate snow accumulation and melt dynamics. Total precipitation, P [mm/t], is divided into liquid (P_{liq}) and solid (P_{sol}) fractions through a temperature-dependent weighting function, defined by lower and upper air temperature thresholds, T_{inf}/ T_{sup} set equal to −0.5°C/0.5°C, that determine pure snowfall and pure rainfall conditions, respectively.

The snowmelt rate, $Snow_{mr}$ [mm/t], is assumed to be proportional to the positive air temperature surplus above the upper air temperature threshold and is controlled by a calibrated degree-day coefficient, Cm [mm/°C/t]. This formulation allows the snow storage to evolve as the balance between snowfall inputs and temperature-driven melt, providing a parsimonious yet physically consistent representation of snow accumulation and ablation processes.

2.1.2. Soil module (S_m)

The soil module simulates water movement in the different layers that comprise the soil. The *MISDc v3.1* model considers a two-layer soil structure, i.e., a superficial and a root zone soil layer (see Fig. 1). The water movement between the layers is governed by two water balance equations involving the surface runoff, the evaporation, the percolation, and the snowmelt.

For superficial (sup) soil layer, the water balance equation can be written as:

$$\begin{cases} \dfrac{dW_{sup}(t)}{dt} = P_{liq}(t) - r(t) - e(t) - g_{sup}(t) + Snow_{mr}(t) \quad W_{sup}(t) \le W_{sup\_max} \\ W_{sup}(t) = W_{sup\_max} \qquad W_{sup}(t) > W_{sup\_max} \end{cases} \tag{1}$$

where W_{sup} [mm] is the water content in superficial layer, P_{liq} [mm/t] is the liquid rainfall from the snow module, r [mm/t] is the surface runoff, e [mm/t] is the evaporation rate, g_{sup} [mm/t] is the percolation between layers, W_{sup_max} [mm] is the total water capacity of the superficial layer.

For root zone (rz) soil layer, the water balance equation is adapted as:

$$\begin{cases} \dfrac{dW_{rz}(t)}{dt} = g_{sup}(t) - g_{rz}(t) - Wuse(t)\ W_{rz}(t) \le W_{rz\_max} \\ W_{rz}(t) = W_{rz\_max}\ W_{rz}(t) > W_{rz\_max} \end{cases} \quad (2)$$

where W_{rz} [mm] is the water content in the root zone, g_{rz} [mm/t] is the deep percolation, W_{use} [mm/t] is the water abstracted for civil/industrial use (see section "Civil and Industrial Water uses Module" for details), W_{rz_max} [mm] is the total water capacity in the root zone layer.

2.1.2.1. Surface runoff. Surface runoff, r, is computed using the equation proposed by Georgakakos and Baumer (1996), which establishes a power-law relationship between r and the soil saturation, $\frac{W_{sup}(t)}{W_{sup\_max}}$, as:

$$r(t) = P_{liq}(t)\left[\frac{W_{sup}(t)}{W_{sup\_max}}\right]^{\alpha} \quad (3)$$

where α [-] is a calibration parameter.

2.1.2.2. Evaporation. Evaporation, e, is calculated by a linear function between the potential evaporation (ET_p) and the soil saturation of the first layer.

$$e(t) = ET_p(t)\frac{W_{sup}(t)}{W_{sup\_max}} \quad (4)$$

The ET_p is estimated based on the Blaney and Criddle relation modified by Doorenbos and Pruitt (1977):

$$ET_p(t) = -2 + b\{\xi[0.46T_a(t) + 8.13]\} \quad (5)$$

where T_a [°C] is air temperature, ξ [-] is the percentage of daytime hours relative to annual total, b [-] is a correction factor for actual evaporation.

2.1.2.3. Percolation. The percolation is modelled through a general equation applicable to both the term referred to the superficial, $g_{sup}(t)$ and root zone $g_{rz}(t)$, soil layer:

$$g(t) = K_s\left[\frac{W(t)}{W_{max}}\right]^{m} \quad (6)$$

where K_s [mm/t] represents the saturated hydraulic conductivity and m [-] is the exponent of the drainage component.

This equation is applied differently for each soil layer by setting K_s equal to $K_{s_{sup}}$ or $K_{s_{rz}}$, m equal to m_{sup} or m_{rz}, and $\frac{W(t)}{W_{max}}$ equal to $\frac{W_{sup}(t)}{W_{sup\_max}}$ or to $\frac{W_{rz}(t)}{W_{rz\_max}}$.

2.1.2.4. Total Runoff Components. Two main components contribute to generate the total runoff: the quick-flow runoff, R_{qf} [mm], mainly related to the surface and shallow-subsurface runoff components (Hu and Li, 2018), and the slow-flow runoff, R_{sf} [mm] produced as an outflow of groundwater storage. These components are estimated according to the following equations:

$$R_{qf}(t) = r(t) + S_{sup}(t) + S_{rz}(t) - \tau\ Vol_{irr}(t) \quad (7)$$

$$R_{sf}(t) = K_{s_{rz}}\left[\frac{W_{sup}(t) + W_{rz}(t)}{W_{sup\_max} + W_{rz\_max}}\right]^{m_{rz}} \quad (8)$$

being r the surface runoff (as in eq. (3)), S_{sup} and S_{rz} [mm] the saturation excess from superficial and root zone soil layer, Vol_{irr} the irrigation volume [mm] as estimated from the "Irrigation Module" (see subsequent section) and τ [-] a coefficient, ranging between 0 and 1, depending on the characteristics of the study basin, representing the portion of Vol_{irr} extracted from superficial water. The saturation excess is evaluated as:

$$\begin{cases} S_{sup}(t) = W_{sup}(t) - W_{sup\_max} \\ S_{rz}(t) = W_{rz}(t) - W_{rz\_max} \end{cases} \quad W_{sup}(t) \ge W_{sup\_max}, W_{rz}(t) \ge W_{rz\_max} \quad (9)$$

By neglecting any lateral flow, the runoff responses at cell scale are averaged at sub-catchment scale to obtain N quick-flow and slow-flow runoff responses, one for each sub-catchment. Specifically, by considering N_C cells for each sub-catchment, the following equations are used:

$$R_{qf,N}(t) = \frac{\sum_{j=1}^{N_C} R_{qf}(t)}{N_C} \quad (10)$$

$$R_{sf,N}(t) = \frac{\sum_{j=1}^{N_C} R_{sf}(t)}{N_C} \quad (11)$$

2.1.3. Civil and industrial water uses module ($CIWU_m$)

The civil and industrial water uses module incorporated in *MISDc v3.1* employed a coefficient-based approach commonly adopted in water utility planning (Maidment and Miaou, 1986; Zhou et al., 2002). Water use can be considered for civil, industrial, or both sectors. First, basic information on typical water consumption per sector is required. The base demand rate (Q_{base}, mm/t) is calculated based on annual total withdrawal volume for civil and industrial sectors. The module can then adjust these values based on various factors like the season and the efficiency of the water system of the study area.

Seasonal variability is incorporated through dimensionless monthly factors (SF) (Hernandez-Samaniego et al., 2023) calculated as the ratio of monthly demand (mm/month) to annual average demand (mm/month) for each sector and month. For civil purposes, intra-annual water use varies significantly because of changing people's daily activities. During summer months, people typically use more water than in winter. For industrial purposes, intra-annual changes are usually smaller because factories tend to use water more consistently year-round. Another feature in the module is the efficiency factor (η), which accounts for water system defects (e.g., some water is lost through leaky pipes, and not all water that enters the system actually reaches the end users). Since water use is not perfectly predictable (e.g., some days people use more water, some days less, depending on weather, events, or just random variation in behaviour), the module includes a random variation to each calculation, up to 10%. The water demand Wuse(t) for each sector at time t is calculated as:

$$W_{use}(t) = \frac{Q_{base} * SF}{\eta} \quad (12)$$

Water use for civil and industrial activities is extracted from the root zone soil layer of the hydrological system, before the estimation of irrigation withdrawals, thus ensuring that essential civil and industrial needs are met first. If the water demands exceed available groundwater, the model records an unmet demand which can be used to assess the water stress conditions in the basin. The advantage of this water use module lies in its flexibility and practicality. This module forecasts water demand without requiring detailed population or economic data inputs, which makes the model more accessible and implementable across different regions where detailed data might be limited.

2.1.4. Irrigation module (I_m)

MISDc v3.1 is integrated with an irrigation module to simulate water withdrawal for irrigation purposes and account its impact on soil moisture and streamflow. Water withdrawal is distributed among various water resources, encompassing surface water, reservoirs as well as root-zone soil layer (see Fig. 1), with a dynamic triggering system based on soil moisture conditions. Specifically, the irrigation scheduling system is operational only during the growing season (e.g., April to September at mid latitude), and it is activated only for the irrigated

pixels (J_{irr}) when the soil saturation of the superficial layer, $\frac{W_{sup}(t)}{W_{sup\_max}}$, falls below a specific threshold (Th_{ini}) set equal to 0.35. Under these conditions, irrigation water is added to the superficial layer to reach a target soil saturation (Th_{irr_sup}) of 0.65. The irrigation water requirement W_{irr} (in mm) for the J_{irr}^{th} pixel, is calculated as:

$$W_{irr,\,J_{irr}}(t) = Th_{irr_{sup}} * W_{sup\_max} - W_{sup,\,J_{irr}}(t) \tag{13}$$

Subsequently, the water content in the J_{irr}^{th} irrigated pixel, is modified as:

$$\begin{cases} \dfrac{W_{sup,Jirr}(t)}{W_{sup\_max}} = Th_{irr_{sup}} & \dfrac{W_{rz,Jirr}(t)}{W_{rz\_max}} > \left[Th_{irr_{sup}} - \dfrac{W_{sup,Jirr}(t)}{W_{sup\_max}} \right] \\ \dfrac{W_{rz,Jirr}(t)}{W_{rz\_max}} = \dfrac{W_{rz,Jirr}(t)}{W_{rz\_max}} - \varepsilon\, W_{irr,\,J_{irr}} & \end{cases} \tag{14}$$

where $\frac{W_{sup,Jirr}}{W_{sup\_max}}$ is the water content in the superficial layer, $\frac{W_{rz,Jirr}}{W_{rz\_max}}$ is the water content in the root zone layer and ε (to be set to a value between 0 and 1, depending on the study basin) indicates the portion of W_{irr} extracted from the root-zone soil layer. This condition holds in the case of available water for irrigation in the root zone layer. Otherwise, only a small percentage of water (here fixed to 10%) is extracted from the root zone soil layer to accomplish irrigation and the soil water content dynamic is described by:

$$\begin{cases} \dfrac{W_{sup,Jirr}(t)}{W_{sup\_max}} = \dfrac{W_{sup,Jirr}(t)}{W_{sup\_max}} + 0.1\dfrac{W_{irr,\,J_{irr}}}{W_{sup\_max}} & \dfrac{W_{rz,Jirr}(t)}{W_{rz\_max}} \\ \dfrac{W_{rz,Jirr}(t)}{W_{rz\_max}} = \dfrac{W_{rz,Jirr}(t)}{W_{rz\_max}} - 0.1\,\varepsilon\, W_{irr,\,J_{irr}} & \\ \leq \left[Th_{irr_{sup}} - \dfrac{W_{sup,Jirr}(t)}{W_{sup\_max}} \right] & \end{cases} \tag{15}$$

This latter condition ensures that water is not completely drained from the root zone soil layer.

The total irrigation volume, Vol_{irr} [mm], counting the total amount of water needed for irrigation in the N^{th} sub-basin, is the sum of the $W_{irr,\,J_{irr}}$ for all the irrigated pixels. It is considered extracted from all the N_C pixels (both irrigated and not irrigated) in the N^{th} sub-basin, over a time span, T_{irr}, of 10 days. Consequently, it is computed as:

$$Vol_{irr}(t) = \sum_{J=1}^{J_{irr}} \frac{W_{irr,\,J_{irr}(t)}}{J_{irr}\,T_{irr}} = \sum_{J=1}^{J_{irr}} \frac{Th_{irr_{sup}} * W_{sup\_max} - W_{sup,\,J_{irr}}(t)}{J_{irr}\,T_{irr}} \tag{16}$$

According to Eq. (7), this irrigation volume does not contribute to generating quick-flow runoff, R_{qf}. However, by updating of the soil water content (see Eq. (14)), it can contribute to the slow-flow runoff, R_{sf} (see Eq. (8)).

2.1.5. Routing module (R_m)

The *MISDc v3.1* model functions in a semi-distributed manner, whereby the entire basin is conceptualised into N sub-basins, which can be classified as either tributary or direct draining areas. The routing module computes river discharge at each sub-basin outlet and transfers it to the basin outlet. In each sub-basin, the quick-flow runoff, R_{qf} component is routed using the geomorphological instantaneous unit hydrograph (GIUH) for tributary areas or a linear reservoir for directly draining areas, while R_{qf} slow-flow runoff component is routed through a linear reservoir. These processes are controlled by a lag-time parameter, dependent on sub-basin area and γ [-] is a parameter to be calibrated. The routed quick and slow-flow components provide the Q_N [m3/s] total discharge at each sub-basin outlet, which is then propagated through the river network to intermediate sections or the basin outlet using a diffusive linear approach defined by diffusivity (D) and celerity (C) parameters.

2.1.6. Reservoir module (Res_m)

The reservoir module implemented in the *MISDc v3.1* model uses the reservoir operation rules as in Burek et al. (2020). These rules are well suited to represent water supply reservoirs operated for flood control and agricultural purposes, which are the most relevant for water resources management. Hydropower reservoirs are not considered in the present implementation, as their operational rules and objectives differ substantially and would require a dedicated representation. The reservoir module is based on the identification of the relative filling, F, i.e., the fraction between the actual storage volume (S) and the total storage capacity ($S_{\max}$), and three filling levels, i.e., the conservative storage limit ($L_c = 0.1$), the flood storage limit ($L_f = 0.9$), and the normal storage limit ($L_n = L_f - L_c$). This module prevents the dam from overtopping during severe flooding by increasing releases to generate a non-damaging outflow when the relative filling exceeds the flood storage limit, thereby keeping storage below the flood control threshold. Consequently, the outflow from the reservoir, Q_{res} ($m^3\,s^{-1}$), is calculated as:

$$\begin{cases} Q_{res} = \min\left(Q_{min}, \dfrac{1}{\Delta t}F.S\right) & F \leq 2L_c \\ Q_{res} = Q_{min} + (Q_{norm} - Q_{min})\left(\dfrac{F - 2L_c}{L_n - 2L_c}\right) & L_n \geq F > 2L_c \\ Q_{res} = Q_{norm} + \dfrac{(F - L_n)}{(L_f - L_n)}.\max\{(I_{res} - Q_{norm}), (Q_{nd} - Q_{norm})\} & L_f \geq F > L_n \\ Q_{res} = \max\left(\dfrac{(F - L_f)}{\Delta t}S, Q_{nd}\right) & F > L_f \end{cases} \tag{17}$$

where F: Reservoir fill, I_{res}: Reservoir inflow ($m^3\ s^{-1}$). The other key parameter is the long-term average inflow to the reservoir, Q_{in_mean}, which regulates the outflow of a reservoir. The outflow thresholds are defined as: minimum outflow ($Q_{min} = 0.4Q_{in\_mean}$), non-damaging outflow ($Q_{nd} = 2Q_{in\_mean}$), and normal outflow ($Q_{norm} = Q_{in\_mean}$).

For the R^{th} reservoir, indicated with *NR_up* and *NR_dw* the number of the upstream and downstream subbasins, respectively, the following water balance equation can be written to update the reservoir storage volumes, S, [m^3] and the reservoir releases, Q_{res} [m^3/s]:

$$\frac{S(t) - S(t-1)}{\Delta t} = \frac{\sum_{N=1}^{NR\_up}[Q_{in}(t-1) + Q_{in}(t)]}{2} - \frac{Q_{res}(t-1) + Q_{res}(t)]}{2} - \frac{\mu \sum_{N=1}^{NR\_dw} Vol_{irr\_NR\_dw}(t)}{\Delta t} \tag{18}$$

where Q_{in} [m^3/s] is the inflow river discharge entering into the reservoir, obtained summing the river discharge from all the *NR_up* upstream sub-basins draining into the reservoir, Δt is the interval time between $(t-1)$ and (t) and μ a coefficient, ranging between 0 and 1 in accordance with the characteristics of the study basin, indicating the portion of irrigation volume extracted from reservoirs. The irrigation term is computed as the sum over all irrigated pixels inside the *NR_dw* subbasins located downstream of the considered reservoir.

For each time step, the model calculates the reservoir releases, Q_{res} through an iterative convergence approach that ensures mass balance. After each iteration, the model recalculates storage and adjusts releases accordingly until convergence is achieved.

2.2. MISDc v3.1 model: input and output data

Data on precipitation, air temperature and water demands for both civil and industrial activities are required by *MISDc v3.1*. As the model has been designed to allow for flexibility with regard to data sources, input data can be provided with either gridded or point sources (e. g.

satellite-derived or in situ) measurements, aggregated at various time steps (from sub-hourly to daily), according to data availability and modelling objectives. If the datasets are characterised by different spatial/temporal resolutions, they need to be resampled over a common spatial grid/temporal time step prior to being used as input for the model.

Furthermore, river discharge time series at selected gauging stations (i.e., outlet and/or inner sections) must be collected, essential for the optimisation of parameters and the evaluation of model performance.

Once calibrated, the model is able to provide estimates of (1) the hydrological storages, i.e., superficial and root zone soil moisture, and snow storage, (2) the fluxes, i.e., actual evaporation, infiltration, percolation, and runoff, and (3) the human components, i.e., irrigation rate, storage and outflow from the reservoirs. Moreover, the river discharge at the closure section of each sub-basin and of the entire basin is provided.

2.3. MISDc v3.1 model: parameters

The model uses 12 calibrated (Cm_{snpack}, α, W_{sup_ini}, W_{rz_max}, m_{sup}, m_{rz}, $K_{s_{sup}}$, $K_{s_{rz}}$, b, γ, C and D) and 9 fixed (T_{inf}, T_{sup}, W_{sup_max}, Th_{ini}, Th_{irr}, η, ε, μ, τ) parameters to simulate the hydrological processes described in section 2.1. Each calibrated parameter varies within a range of values (see Table 1) derived through physical reasoning and extensive application of previous versions of the *MISDc* model in numerous catchments (Massari et al., 2015; Masseroni et al., 2017; Camici et al., 2018, 2025; Cislaghi et al., 2020). Similarly, the values of T_{inf}, T_{sup}, W_{sup_max}, Th_{ini}, Th_{irr} are defined through a tuning phase and validated through the extensive application of previous *MISDc* model versions in different catchments (Cislaghi et al., 2020; Camici et al., 2025). The remaining fixed parameters ($\eta, \varepsilon, \mu, \tau$) are set according to the characteristics of the specific study area.

2.4. MISDc v3.1 model: calibration and validation

The *MISDc v3.1* model can be calibrated through a sequential calibration, i.e., by considering the river discharge observed at multiple inner sections, from upstream to downstream, as well as at the outlet section of the entire basin (De Lavenne et al., 2019). When this sequential procedure is applied, distinct model parameter sets are obtained for each section. The calibrated parameters are set by minimising an objective function based on the modified Kling-Gupta efficiency (Kling et al., 2012) index. It ranges from -∞ to 1, where 1 indicates a perfect agreement between simulations and observations.

2.5. Model uncertainty characterization: the BLUECAT approach

In order to assess uncertainty of *MISDc v3.1* river discharge model predictions, the BLUECAT method is applied here (Koutsoyiannis and Montanari, 2022; Montanari and Koutsoyiannis, 2025). BLUECAT converts deterministic model predictions into a probabilistic framework, enabling both bias correction and quantification of predictive uncertainty. BLUECAT derives the probability distribution of the target variable directly from the statistical relationship between model outputs and observations, rather than relying on assumptions about the structure of prediction errors. The approach first estimates the conditional probability distribution of the true variable to be predicted depending on the outcome from the deterministic prediction, and then uses this distribution to produce bias-corrected forecasts together with confidence intervals. This formulation allows BLUECAT to seamlessly integrate deterministic modelling whether physically based or data-driven with a stochastic representation that is both theoretically rigorous and transparent in its use of data. In the present application, the stochastic forecast corresponds to the mean of the estimated predictive probability distribution, while the confidence interval is computed with a significance level of 0.2, which corresponds to a confidence level of 80%.

3. Study area

The Po River constitutes the most extensive hydrographic basin in Italy, encompassing an area of 72,000 km^2 and a total river length of 652 km. This river system, fed by 141 tributaries, extends from the western border of northern Italy to its eastern border, and from the Alps in the north to the Apennine Mountains in the south, thereby demonstrating its substantial hydrological complexity and significance within the Italian landscape.

The average annual rainfall of the basin is 1030 mm, and the average annual flow (2000-2023) at Pontelagoscuro station is 1395 m^3/s. The annual average temperature varies between 5°C and 15°C, around 5°C in the high Alps, 5–10°C in the medium-height mountains, and 10–15°C in the other zones (Vezzoli et al., 2015; Musolino et al., 2018; Formetta et al., 2022). The hydrological system of the basin is very complex with

Table 1
Parameters of the *MISDc v3.1* hydrological model, derived by calibration (calibrated parameters) or fixed a priori (fixed parameters). For each of them, a description is provided.

Calibrated parameter	Description	Module	Variability range	Unit
Cm_{snpack}	degree-day coefficient for snowpack	Snow	0.004-3	[-]
α	exponent of runoff	Soil	1-30	[-]
W_{sup_ini}	initial condition of the water content in the superficial layer	Soil	0.1-0.9	[-]
W_{rz_max}	total water capacity of the root zone soil layer	Soil	300-4000	[mm]
m_{sup}	exponents of drainage for the superficial soil layer	Soil	2-10	[-]
m_{rz}	exponents of drainage for the root zone soil layer	Soil	5-20	[-]
$K_{s_{sup}}$	hydraulic conductivity for the superficial soil layer	Soil	0.10-20	[mm h^{-1}]
$K_{s_{rz}}$	hydraulic conductivity for the root zone soil layer	Soil	0.01-45	[mm h^{-1}]
b	correction factor for actual evaporation	Soil	0.4-2	[-]
γ	lag-time parameter	Routing	0.5-3.5	[-]
C	Celerity	Routing	1-60	[km h^{-1}]
D	Diffusivity	Routing	1-30	[km^2 h^{-1}]
Fixed parameter	**Description**	**Module**	**Set value**	**Unit**
T_{inf}	air temperatures below which all precipitation falls as snow	Snow	−0.5	[°C]
T_{sup}	air temperatures above which all precipitation falls as rain	Snow	0.5	[°C]
W_{sup_max}	total water capacity of the superficial soil layer	Soil	200	[mm]
Th_{ini}	threshold for activation of irrigation module	Irrigation	0.3	[-]
Th_{irr}	threshold for termination of irrigation module	Irrigation	0.5	[-]
ε, μ, τ	Percentage of irrigation water extracted from superficial water, root-zone layer, and reservoirs	Soil/Irrigation/ reservoir	17%, 80%, 3%	[-]

various hydroclimatic regimes: (1) the Alpine reaches, which are snow-dominated and receive water primarily from snow and glacial melt, exhibiting a characteristic seasonal peak between spring and early summer, (2) the Apennine rivers, which are rainfall-dominated, presenting a minimum seasonal flow during the summer, and (3) the Pianura Padana plain, where flows are more stable, moderated by upstream contributions, lakes, and irrigation channels, making this zone vital for agriculture and water management. The basin contains a dense network of 174 reservoirs and lakes, primarily constructed for hydropower generation (Evangelista et al., 2025), which contribute to the region's complex hydrological system with a total storage volume of approximately 2.20 km^3 (https://suwanu-europe.eu/wp-content/uploads/2021/05/State-of-play_Po-River-Basin-Italy.pdf). In this study, the four largest regulated lakes i.e., Maggiore, Como, Iseo, and Garda are considered. Together, they provide a total storage volume of approximately 1.30 km^3, representing about 60% of the basin's total reservoir and lake storage. Their outflows are regulated by outlet barrages located at Miorina, Olginate, Sarnico, and Salionze, respectively, which control lake releases to support irrigation and industrial water supply, as well as to enhance flood attenuation within the basin. Spatial distribution of these lakes within the basin is shown in Fig. 2.

4. Input data

4.1. Meteorological data

The meteorological forcing comprises precipitation and air temperature data. Daily high-resolution (5 km, 1981-2023) gridded precipitation data is obtained from the ArCIS dataset (Pavan et al., 2019), generated by interpolating in situ observed data from a high-density climate monitoring network over north-central Italy.

Daily high-resolution (4 km, 2000–2023) surface air temperature (T2m) data are obtained from the UniMi/ISAC-CNR observational dataset (Cavalleri et al., 2024). The dataset is constructed from homogenized minimum and maximum temperature records and interpolated using an anomaly-based approach (Mitchell and Jones, 2005; Brunetti et al., 2012), ensuring consistency over complex terrain.

4.2. Hydrological data

Daily river discharge (2000–2022) is obtained from the Italian Civil Protection Department (DPC) and the Po River Basin Authority (ADBPO) for 18 gauge stations (six along the main stream and twelve uniformly scattered throughout the tributaries of the Po River, as illustrated in Fig. 2 and detailed in Table S1). In addition, for Maggiore, Como, Iseo, and Garda lakes, daily time series of water storage volume and outflow are provided by ADBPO for the period 2000-2022.

4.3. Water use data

Data related to water uses for civil and industrial purposes over the study area is collected from the Po River Basin Management Plan (PdgP, 2010; 2016) prepared by ADBPO. Total withdrawals amount to ~4 $km^3\ yr^{-1}$, corresponding to 0.133 and 0.089 mm/d at basin scale for civil and industrial uses, respectively. When compared with the mean annual precipitation over the study area (1030 mm/y), these withdrawals represent approximately 5.3% of the total annual precipitation. For the study area, on average about 30% of withdrawals of water for civil and industrial purposes is lost during distribution (Klabunde et al., 2025). Consequently, Q_{base} and η and in the water use module are set to 0.15 mm/d and 30%, respectively.

Agricultural water use is provided by ADBPO, based on data

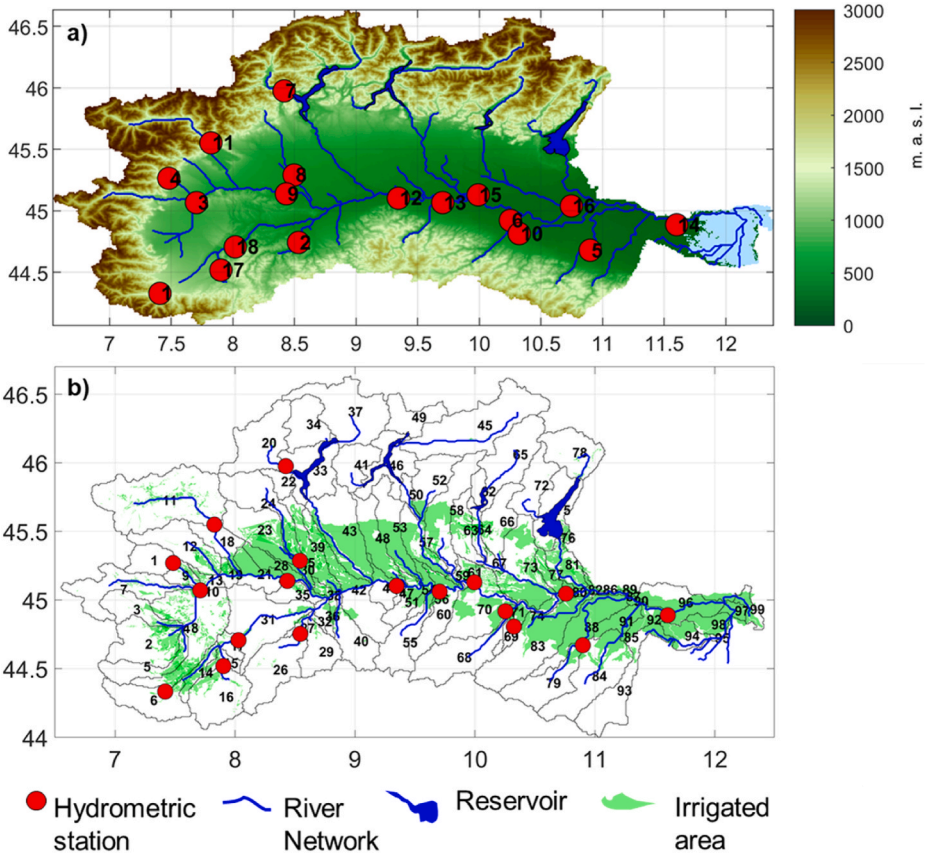

Fig. 2. Po River basin. (a) Main river network and location of the river discharge gauging stations. (b) Identification of *N* sub basins, *R* reservoirs and the *Jirr* irrigated areas (extracted from SIGRIAN database) in the study area.

collected from the National Information System for the Management of Water Resources in Agriculture (SIGRIAN; https://sigrian.crea.gov.it/index.php/en/home-3/). This database serves as a comprehensive repository, aggregating information at district level on natural resource management, irrigation infrastructure, and agronomic practices associated with collective irrigation at the national level. For the Po River basin, data is available at annual scale from 2016 to 2021. On average, approximately 12 km^3 of water is utilised yearly for irrigation purposes, which is equivalent to 0.53 mm/d at basin scale. This volume accounts for approximately 19% of the mean annual precipitation over the study area. As shown in Fig. 2b, the SIGRIAN database also provides information regarding the distribution of irrigated areas.

Finally, irrigation supply is assumed to originate from surface water (80%), groundwater (17%), and reservoirs (3%), consistent with Berselli (2022), Bozzola and Swanson (2014) and the PdgP (2010 and 2016). These fractions are considered spatially uniform over the basin and temporally constant over the simulation period due to the lack of higher-resolution source-specific data. Accordingly, the corresponding *MISDC v3.1* parameters controlling irrigation source allocation (τ, ε, and μ) are set to 0.80, 0.17, and 0.03, respectively.

4.4. Additional high-resolution datasets

High-resolution satellite-based datasets are used to validate the hydrological model estimates. The datasets include potential evapotranspiration, surface and root zone soil moisture, snow water equivalent and irrigation water use data. The details of each dataset are given in Table 2.

Table 2
Details of datasets collected over the Po study area.

	Hydrological variable (available period)	Source	Type of data	Spatial/ Temporal resolution
Meteorological Data	Precipitation (2000-2023)	ArCIS dataset (Pavan et al., 2019) http://www.arcis.it/	In situ	5km/1day
	Air Temperature (2000-2023)	UniMi/ISAC-CNR observational dataset (Cavalleri et al., 2024)	In situ	4km/1day
Hydrological Data	River Discharge (2000-2022)	Italian Civil Protection Department and the Po River Basin Authority	In situ	Daily
	Reservoir Storage Volume and Outflow (2003-2020)	Po River Basin Authority	In situ	Daily
Water Use Data	Water Use for Civil and Industries (2010 and 2018)	Po River Basin Management Plan (PdgP, 2010; 2016)	In situ	Monthly
	Water Use for Agriculture (2016-2021)	Po River Basin Authority (SIGRIAN, https://sigrian.crea.gov.it/index.php/en/home-3/)	In situ	Annual
Additional Datasets	Potential Evaporation and Surface and Root Zone Soil Moisture (2003-2022)	GLEAM v3.7b (GLEAM, Miralles et al., 2011; Martens et al., 2017) https://www.gleam.eu/	Modelled with Satellite data assimilation	1km/1day
	Snow Water Equivalent (2011-2021)	Avanzi et al. (2022) https://stac.eurac.edu:8080/?.language=en	Snow reanalysis for Italy blending modeling, in situ data, and satellite observations	1km/1day
	Irrigation data v1.0 (2016-2020)	Dari et al. (2023) https://doi.org/10.5281/zenodo.7341284	Satellite-based data	1km/7 day

5. Modelling setup and experimental analysis

5.1. Modelling setup

To run, the *MISDc v3.1* must be properly configured for the study area. This encompasses: (1) the definition of the river network topology, i.e., the way pixels, sub-basins, reservoirs and streams are interconnected with each other and with the basin outlet; (2) the preparation of the input data and (3) the model calibration. Because this setup procedure is applied consistently across all study areas, a general description of the workflow is provided below, followed by its implementation for the Po study basin.

The topological structure of the basin is defined using topographic data (e.g., SHuttle Elevation Derivatives at multiple Scales, HydroSHEDS, DEM, https://www.hydrosheds.org/), as well as the location of points of interest such as river discharge monitoring stations (derived e.g., from the Global Runoff Data Centre, https://grdc.bafg.de/, GRDC, 2020), and reservoirs (location and storage capacity derived from e.g., Global Reservoir and Dam Database v1.3, GRanD v1.3, Lehner et al., 2011). Based on these datasets and following the delineation procedure described by Camici et al. (2022), the study basin is divided into N sub-basins. River network nodes associated with reservoirs and lakes (R nodes) are incorporated using an approach similar to that proposed by Han et al. (2023). To identify the irrigated (*Jirr*) pixels within each sub-basin, information on irrigated lands can be obtained by local authorities or can be derived using global dataset of areas equipped for irrigation (e.g., Siebert et al., 2015; Kebede et al., 2025) or regional satellite-based irrigation estimates (e.g., Dari et al., 2023).

Accordingly, *MISDc v3.1* is implemented for the Po River basin. Based on the derived river network topology and the spatial distribution of the 18 river gauge stations, the basin is delineated into 99 sub-basins (Fig. 2b). Reservoir representation includes the major regulated lakes in Northern Italy namely Lake Maggiore, Lake Como, Lake Iseo, and Lake Garda, which play a dominant role in regional water regulation and irrigation supply. Smaller reservoirs and hydropower-dominated alpine systems are not included; their effects are therefore not explicitly represented in the model. To identify pixels, and consequently the sub-basins, where irrigation typically occurs within the Po basin, the SIGRIAN district dataset is used (see Fig. 2b). A pixel is classified as irrigated if more than 50% of its area falls within a SIGRIAN-designated irrigated district. The irrigation module within the *MISDc v3.1* model is then activated for the *Jirr* pixels, during the April-September growing period.

Concerning the meteorological input, precipitation and air temperature data must be extracted for each of the N sub-basins. In the Po case study, differences in spatial resolution and temporal coverage among the gridded meteorological datasets require an initial resampling to a common 5 km spatial grid and 1-day temporal resolution. The analysis period is set to 2000–2023, corresponding to the longest common period across the input datasets (see Section 4.2). The resampled data are then

extracted for each of the 99 sub-basins.

Once the model structure is defined, the *MISDc v3.1* model parameters are calibrated. For the Po case study, among the available 18 river gauge stations, 4 stations i.e., Pontelagoscuro, Spessa, Borgoforte, and Casale Monferrato, all located along the main reach, are used for model calibration for the period of 2000–2022. The model is calibrated sequentially from upstream to downstream for these 4 sections, yielding four distinct parameter sets, one for each calibrated section.

Then, *MISDc v3.1* model can be used to simulate, for each of the *N* sub-basin, streamflow, soil moisture in the superficial and root zone layers, snow dynamics, irrigation water withdrawal as well as storage and outflow dynamics for the *R* reservoirs. These simulated variables can be independently validated to demonstrate the model's suitability in reproducing the entire hydrological cycle. For the Po case study, 14 out of 18 gauging stations are used for validation purposes (see Table S1).

5.2. Experimental analysis

The experimental analysis aims to comprehensively evaluate the performance of the modelling framework in reproducing hydrological dynamics across the Po River basin. First, the ability of the model to simulate streamflow at multiple sections of the study basin is assessed. Both calibrated and non-calibrated gauging stations are considered to test model transferability and generalization capability. The evaluation focuses on the reproduction of the complete river discharge time series as well as on the model's ability to capture extreme events. For the Po case study, the analysis is focused on the 2002, 2014, and 2019 flood events and 2012, 2017, and 2022 drought events. Moreover, river discharge uncertainty is quantified using the BLUECAT tool.

Second, the consistency of the model in representing the main components of the hydrological cycle, both natural and anthropogenic is analyzed. The assessment is conducted at a daily scale by aggregating variables over different sub-basins (closed at Casale Monferrato, Cremona, and Pontelagoscuro sections), and at a seasonal scale by aggregating data across major hydrological compartments (i.e., Alpine, Apennine and Pianura Padana, see Fig. S2) within the Po basin. In particular, in the validation multiple hydrological variables such as soil moisture, evaporation estimates, snow water equivalent, lake storage and outflow dynamics, and irrigation volumes are compared against the high-resolution datasets described in Table 2. In addition, an annual water balance analysis is conducted to assess long-term mass conservation and flux partitioning at the basin scale. For each year, precipitation and irrigation inputs are compared with evapotranspiration, outlet runoff, anthropogenic withdrawals, and storage changes in soil, snow, groundwater, lakes, and reservoirs. This evaluation verifies basin-scale water balance closure and clarifies the relative contribution of natural and human processes to interannual variability. By combining daily, seasonal, and annual diagnostics, the multi-scale framework ensures a comprehensive evaluation of internal process consistency under varying hydro-climatic conditions.

Finally, the impact of anthropogenic modules on streamflow simulation is explicitly evaluated. Comparative analyses quantify how the inclusion of human-related processes (e.g., regulation, withdrawals and irrigation) influences river discharge dynamics and the representation of extreme events. This step isolates the contribution of anthropogenic components and assesses their added value in improving model realism and predictive capability.

Model performance across alternative configurations is evaluated using the KGE', Nash–Sutcliffe Efficiency (NS, Nash and Sutcliffe, 1970), and Pearson correlation coefficient (rc, Pearson, 1895). These metrics are not suitable for cross-site comparisons, as their values are influenced by the variability of streamflow at each station (Williams, 2025; Knoben et al., 2019). To enable cross-site evaluation, the Normalized Root Mean Square Error (nRMSE; Abdelkader et al., 2023) is used. The nRMSE ranges from 0 to ∞, with 0 indicating perfect agreement, providing a scale-independent measure of model error for direct comparison across stations with different flow regimes. All metrics are computed at the daily scale.

6. Results

6.1. River discharge modelling

River discharge at calibrated sections (Pontelagoscuro, Spessa, Borgoforte, Casale Monferrato) for the time period 2000-2023, together with a detailed view of Jan–May, 2020 is shown in Fig. 3. Over the simulation period, the model exhibited consistently strong performance at Pontelagoscuro, Spessa, and Borgoforte. High KGE' values (KGE' = 0.89–0.93) and NS values (NS = 0.79–0.87), together with strong correlation coefficients (rc = 0.90–0.93), indicate that the model accurately captured both the temporal variability and the magnitude of river discharge at each site. The relatively consistent nRMSE values (nRMSE = 31%-33%) across these sections showed stable model behaviour in reproducing flow dynamics over a wide range of hydrological conditions. At Casale Monferrato, model performance is comparatively weaker, with an error magnitude (nRMSE) of 47%, but the correlation coefficient is high (rc = 0.93), indicating that the timing and general variability of flows are well represented. The zoomed view for Jan–May 2020 provided further insight into the model's capability to reproduce short-term hydrological dynamics. At Pontelagoscuro, Spessa, and Borgoforte, the model successfully captured the seasonal recession during winter and the subsequent rise in river discharge during spring, including the timing and amplitude of peak flows. Performance metrics remained robust (nRMSE = 18%-26%) in this short-term evaluation, but at Casale Monferrato, performance declined more noticeably (nRMSE = 49%), indicating greater sensitivity to short-term fluctuations and potentially to localized hydrological processes.

Calibration and performance metrics of *MISDc v3.1* model for all gauge sections across the basin are summarized in Table 3 for calibrated and validated sections over the main river and tributaries. The hydrological model demonstrated superior performance for the validated sections on the main river compared to tributary sections (see Table S1 for the location of the stations). The model also showed strong skills in reproducing both the timing and magnitude of extreme hydrological events across multiple years. Fig. 4 presented the river discharge time series for the flood events of 2019, 2014, and 2002, as well as for the drought periods of 2022, 2017, and 2012. The quantitative evaluation of model performance during these extreme hydrological events indicated overall good agreement with observations. During flood events, the model achieved nRMSE values ranging from 20% to 39% across all sections, accurately capturing both the timing and magnitude of flood peaks. The drought events of 2017 and 2012 are also simulated with good performance, with nRMSE values between 25% and 41%. However, model accuracy declined under the exceptionally severe low-flow conditions observed during the 2022 drought, with nRMSE values increasing to 41%–71%.

6.2. Model uncertainty evaluation

The uncertainty in *MISDc v3.1* river discharge predictions is assessed using the BLUECAT method. Specifically, the BLUECAT-corrected river discharges are compared with observed data at the four calibrated stations (Pontelagoscuro, Spessa, Borgoforte, and Casale Monferrato) (Fig. 5). Values of *r,* NSE and KGE' with and without BLUECAT correction for the period 2000-2023 are given in Table 4, along with the percentage of observed lying within the confidence at significance level of 0.2. In all stations except for Spessa, the BLUECAT correction improved the accuracy of the original deterministic simulations, according to *r* and NSE. However, lower values of KGE' are found at all stations except Casale Monferrato. The percentage of points lying within the confidence bands is close to 70%, thus confirming that uncertainty is correctly estimated. The decrease in KGE' is primarily due to changes in

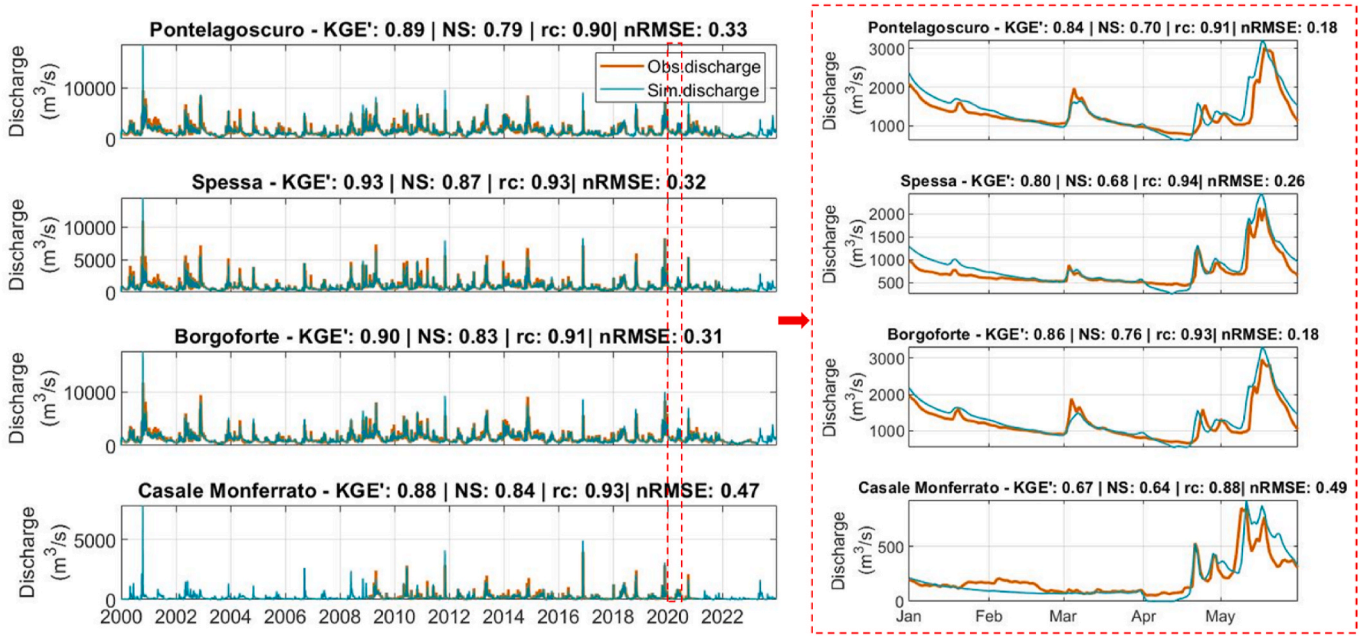

Fig. 3. Observed and simulated river discharge at calibrated sections (Pontelagoscuro, Spessa, Borgoforte, Casale Monferrato). The left panels show a time series from 2000 to 2023, whereas the right panels present a detailed view of Jan 2020 –May 2020.

Table 3
Performance metrics of *MISDc v3.1* model for all gauging sections across the Po River basin. Calibrated sections are indicated in bold.

ID station	Name station	KGE'	NS	*rc*	*nRMSE*
1	Stura di Demonte@Gaiola	−0.34	−4.05	0.77	2.03
2	Bormida@Cassine	−0.12	0.23	0.63	2.18
3	Po@Torino Murazzi	0.54	0.71	0.88	0.64
4	Stura di Lanzo@Lanzo	0.49	0.66	0.87	0.75
5	Secchia@Ponte Alto	0.76	0.67	0.82	1.05
6	Taro@S. Secondo	−1.78	−3.91	0.68	3.90
7	Toce@Candoglia	0.71	0.47	0.72	0.84
8	Sesia@Palestro	0.41	0.39	0.69	1.49
9	**Po@Casale Monferrato**	**0.90**	**0.81**	**0.91**	**0.57**
10	Parma@Ponte Verdi	0.27	0.37	0.62	1.98
11	Dora Baltea@Tavagnasco	0.29	0.40	0.84	0.65
12	**Po@Spessa**	**0.93**	**0.87**	**0.93**	**0.32**
13	Po@Piacenza	0.92	0.86	0.93	0.32
14	**Po@Pontelagoscuro**	**0.89**	**0.79**	**0.90**	**0.33**
15	Po@Cremona	0.91	0.87	0.94	0.29
16	**Po@Borgoforte**	**0.90**	**0.83**	**0.91**	**0.31**
17	Tanaro@Farigliano	0.50	0.48	0.70	1.18
18	Tanaro@Alba Q.A.	0.46	0.52	0.79	0.90

the bias ratio (β) and variability ratio (δ) (Table 5). After BLUECAT correction, both β and δ deviate further from their optimal value (1) in most sections, except for Casale Monferrato, where β improves. The lower values of KGE' are explained by less reliable simulation of mean value and variability after BLUECAT correction. In fact, BLUECAT corrects the bias across the whole range of quantiles and typically the magnitude of the correction is larger for higher flows. The adjustment of the latter ensures a better performance in terms of quadratic goodness of fit statistics like NSE and *r*, while possibly lowering the score of non-quadratic measures like the bias of the mean simulation.

6.3. Model validation across sub-basins and hydrological compartments

6.3.1. Soil moisture, evapotranspiration, snow water equivalent modelling

The *MISDc v3.1* model is validated against key hydrological variables, including soil moisture, evaporation, and snow water equivalent. The assessment is conducted at a daily scale by aggregating variables over different sub-basins at Casale Monferrato and Cremona sections (Fig. S1), and at Pontelagoscuro section (Fig. 6). Seasonal variability is evaluated by averaging monthly values of soil moisture (2003–2022), evaporation (2003–2022), and snow water equivalent (2011–2021) across Apennine, Alpine, and Pianura Padana regions (Fig. S2). High-resolution datasets are used as independent references to verify that the model adequately reproduces internal hydrological processes. At Casale Monferrato and Cremona sections, the soil moisture simulation reproduced the magnitude well, with nRMSE values of 24% (Casale Monferrato) and 17% (Cremona) for the superficial layer, and 6% (Casale Monferrato) and 5% (Cremona) for the root-zone layer; however, the temporal pattern is not well captured. At Pontelagoscuro, the model performed very well in simulating soil moisture in both the superficial and root-zone layers, with nRMSE values of 17% and 4%, respectively. The simulated soil moisture closely followed the temporal dynamics and seasonal fluctuations observed in the GLEAM dataset over the 20-year period, accurately capturing both wet and dry phases. The model satisfactorily reproduced the seasonal dynamics of soil moisture in the Apennine and Pianura Padana regions, accurately capturing the timing and amplitude of the winter recharge and summer depletion phases (See Fig. S2a and S2b). Seasonality is stronger in the Apennine region, where the model represented pronounced summer drying and high winter storage, while the Pianura Padana region exhibited more moderate variability. In the Alpine region, the model captured the overall seasonal pattern but showed a negative bias in surface soil moisture during winter and early spring.

Evaporation simulations showed reasonable agreement with the GLEAM dataset across all three sections, with nRMSE values of 37% at Casale Monferrato, 44% at Cremona, and 35% at Pontelagoscuro. Both simulated and GLEAM evaporation exhibited consistent seasonal oscillations, ranging approximately from 0 to 4 mm/d, with peak evaporation occurring during summer and minimum values during winter. In Appennine, Alpine, and Pianura Padana regions, evaporation is characterized by a well-defined seasonal cycle, with peak values in late spring–summer (See Fig. S2c). Although the phase of the seasonal cycle is well reproduced, the model showed smaller values than GLEAM in warm-season in all regions, indicating a residual bias in growing-season fluxes.

For snow water equivalent, the modelled values showed strong

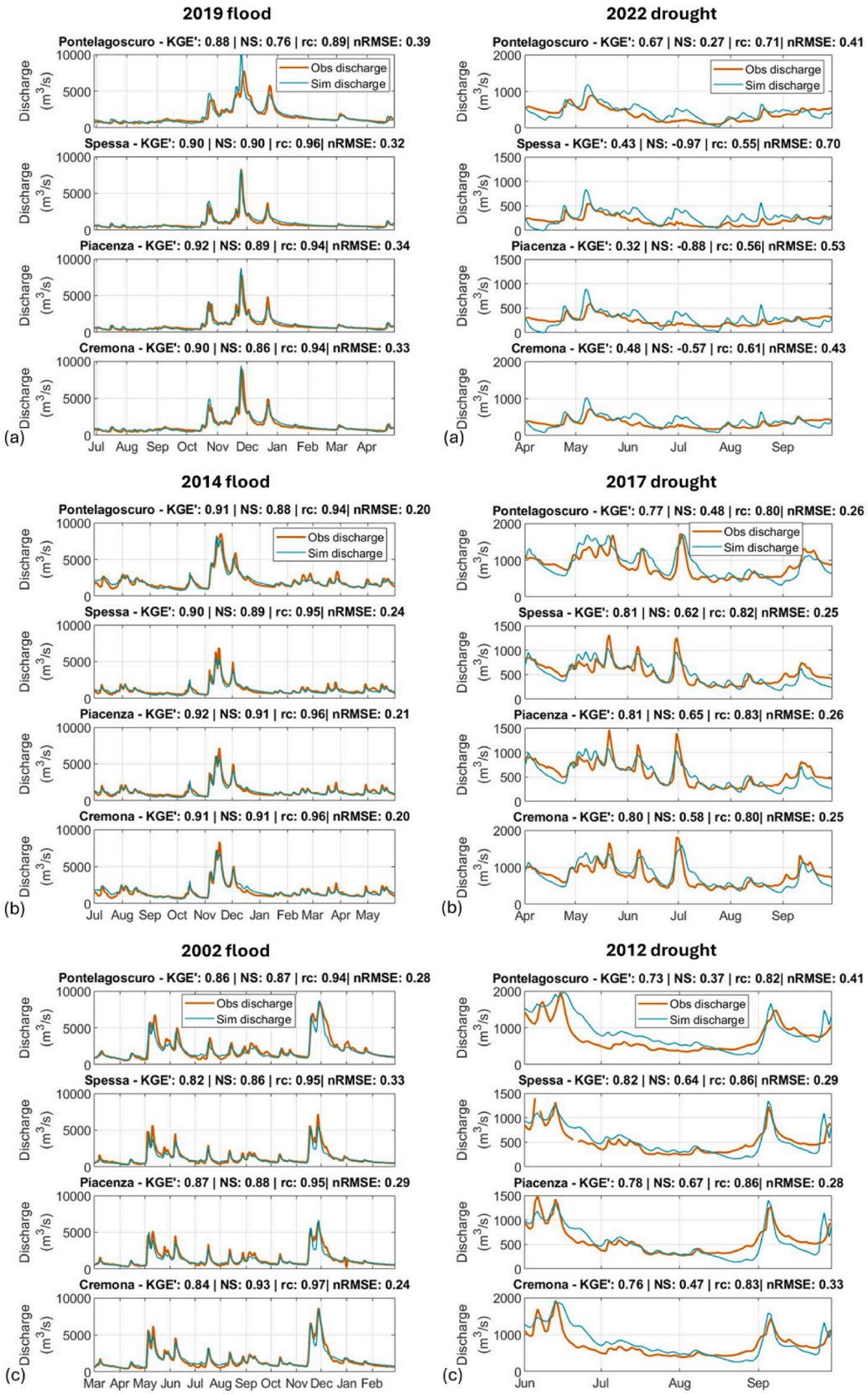

Fig. 4. Extreme hydrological events at Pontelagoscuro (calibrated), Spessa (calibrated), Piacenza (uncalibrated) and Cremona (uncalibrated) sections located on the main reaches of the Po River. The left Panels illustrate flood events in 2019 (plot a), 2014 (plot b), and 2002 (plot c), while the right panels show drought events in 2022 (plot a), 2017 (plot b) and 2012 (plot c).

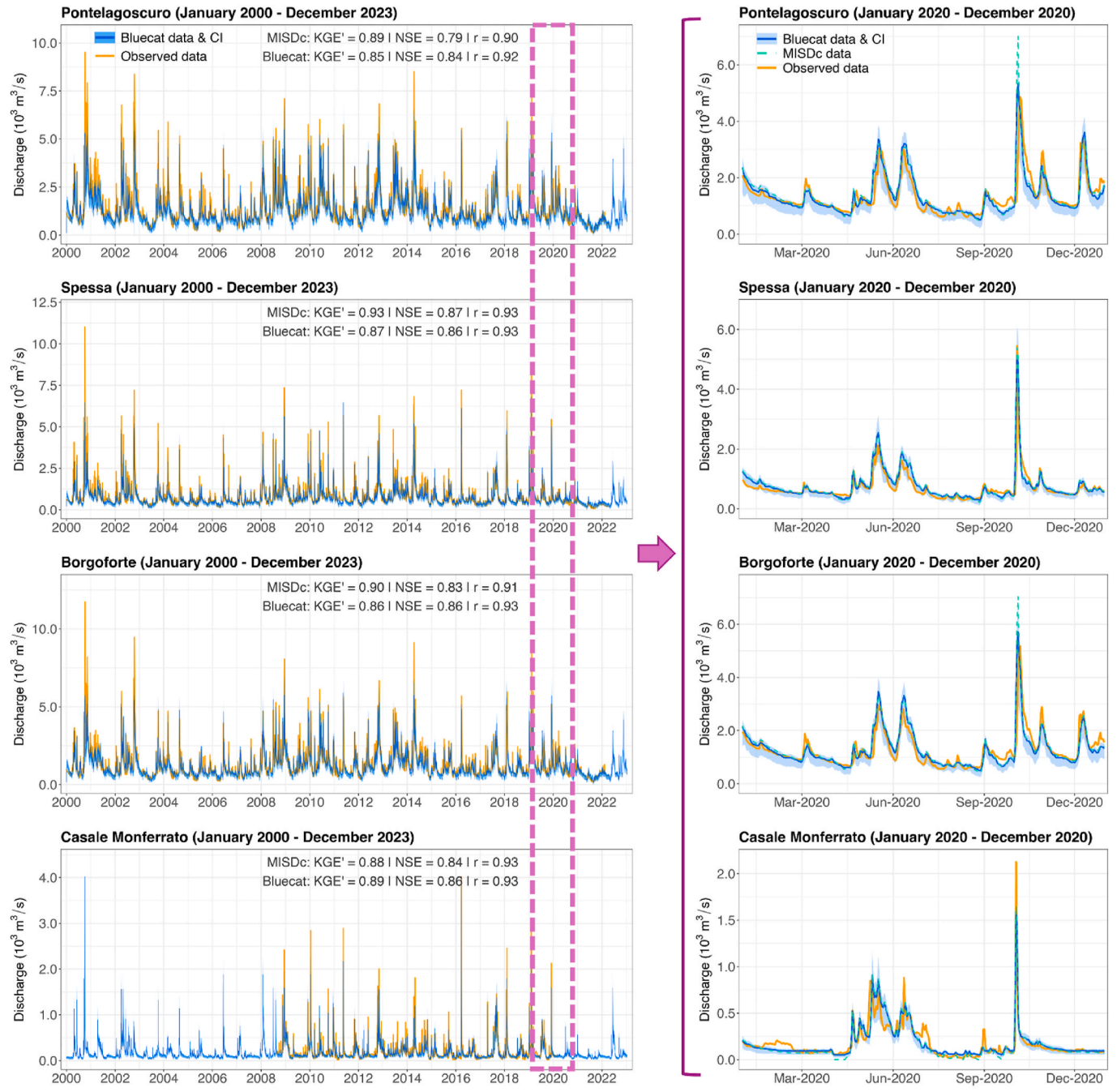

Fig. 5. Comparison between observed discharge and *MISDc v3.1*-simulated discharge after correction with the BLUECAT method across the four calibrated sections. The left panels show time series from 2000 to 2023, while the right panels provide a zoom on the period January 2020–December 2020. The zoomed -period plots display both original *MISDc v3.1* simulations and *MISDc v3.1* simulations after BLUECAT correction. The left panels also show performance metrics comparing the original and BLUECAT-corrected simulations against observations over the whole 2000–2023 time series.

Table 4
Performance metrics of *MISDc v3.1* simulated streamflow before and after BLUECAT stochastic correction. The table reports the Pearson correlation coefficient (r), Nash–Sutcliffe Efficiency (NSE), modified Kling–Gupta Efficiency (KGE'), and the percentage of observed flows falling within the Bluecat 80% confidence interval (Obs in CI) for each river section.

Section	*r* MISDc	*r* BLUECAT	*NSE* MISDc	*NSE* BLUECAT	*KGE'* MISDc	*KGE'* BLUECAT	Obs in CI [%]
Pontelagoscuro	0.90	0.92	0.79	0.84	0.89	0.85	69.20
Spessa	0.93	0.93	0.87	0.86	0.93	0.87	70.80
Borgoforte	0.91	0.93	0.83	0.86	0.90	0.86	70.60
Casale Monferrato	0.93	0.93	0.84	0.86	0.88	0.89	69.20

Table 5
Components of the modified Kling–Gupta Efficiency (KGE') for *MISDc v3.1* simulated streamflow before and after Bluecat stochastic correction. The table reports the correlation coefficient (r), bias ratio (β), and variability ratio (δ) for each river section, allowing assessment of which component contributes most to KGE' changes after the Bluecat application.

Section	r MISDc	r BLUECAT	β MISDc	β BLUECAT	δ MISDc	δ BLUECAT
Pontelagoscuro	0.90	0.92	1.01	0.98	0.98	0.84
Spessa	0.93	0.93	0.98	0.97	0.97	0.87
Borgoforte	0.91	0.93	1.01	1.00	0.97	0.86
Casale Monferrato	0.93	0.93	0.98	1.00	1.07	0.92

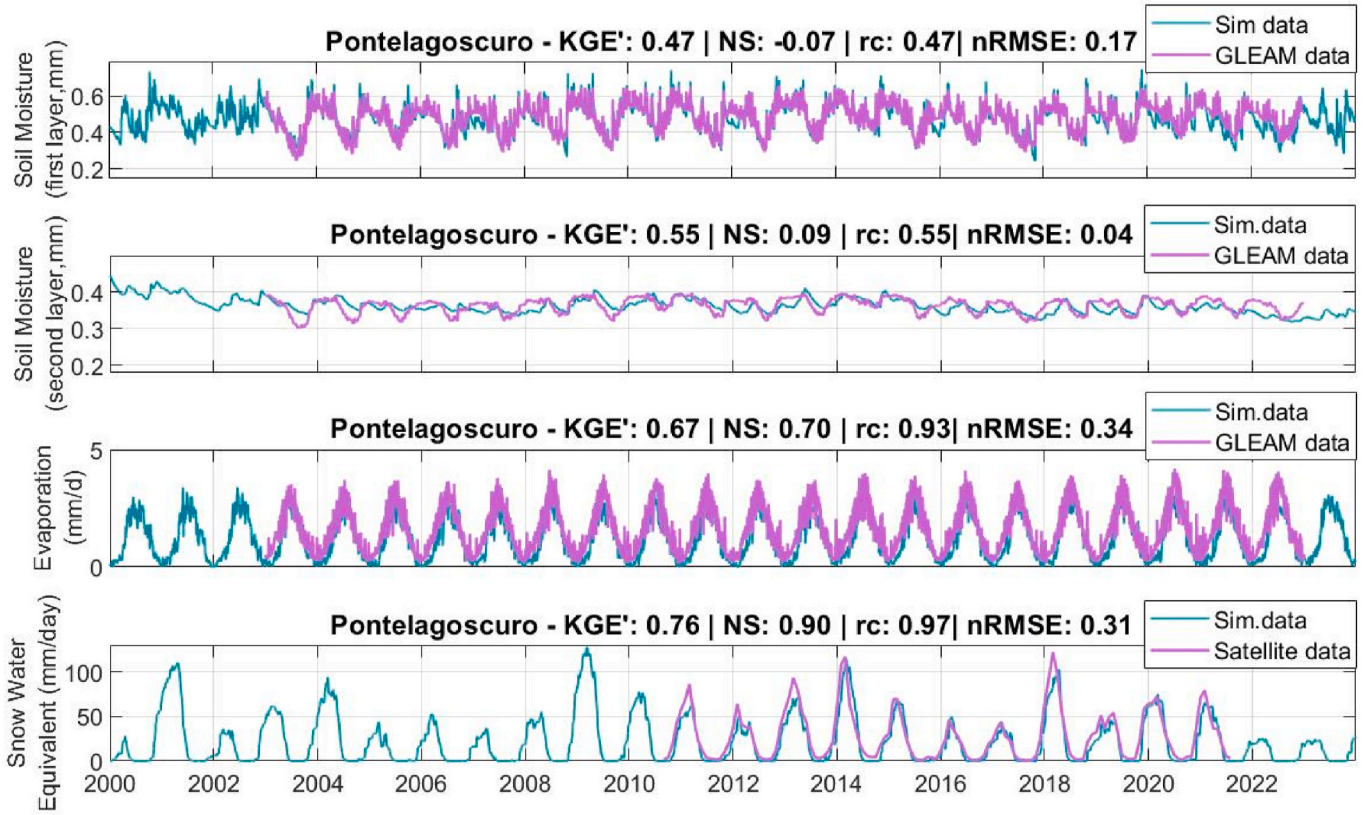

Fig. 6. Comparison between observed and simulated superficial and root zone soil moisture (plot a and plot b, respectively), evapotranspiration (plot c) and snow water equivalent (plot d) at Pontelagoscuro section (i.e., the closure section of the Po River basin).

agreement with satellite based observations over the period 2011–2021 at Casale Monferrato, Cremona, and Pontelagoscuro sections. The model successfully reproduced the pronounced seasonal accumulation and melt cycles, with peak snow water equivalent ranging from approximately 50 to 300 mm. This indicates that the model adequately captured snow accumulation and ablation processes, which are critical for spring and early summer runoff generation. Snow water equivalent is negligible in the Apennine and Pianura Padana regions (See Fig. S2d). In contrast, the Alpine region showed substantial winter accumulation, and the model closely reproduced both the magnitude and timing of snow storage and melt, supporting the robustness of the cryospheric representation.

6.3.2. *Reservoir modelling*

The performance of reservoir simulation is evaluated based on the model's ability to reproduce lake storage volumes and outflow discharges for Lakes Maggiore, Como, Iseo, and Garda over the period 2003–2020 (Fig. 7). For Lake Maggiore, the model reproduced storage and outflow dynamics with nRMSE values of 35% and 48%, respectively. While the temporal evolution of lake storage is well captured, peak storage volumes are underestimated, particularly in 2004 and 2014. Lake Como exhibited the poorest performance in storage simulation among all lakes, with an nRMSE of 59%, reflecting a systematic overestimation of storage volumes throughout most of the simulation period. In contrast, outflow simulation showed better performance (nRMSE = 38%), indicating that the model captures regulated releases more accurately than storage dynamics for Lake Como. Lake Iseo demonstrated good performance in simulating both storage and outflow, with nRMSE values of 34% and 43%, respectively. The model effectively captured the seasonal storage patterns, although it tends to overestimate lower storage volumes during 2014–2020. Lake Garda demonstrated moderate storage simulation performance, capturing major storage volumes while overestimating lower volumes during severe drawdown periods (2003-2007, 2014-2017). Outflow simulation showed poor performance, with the model unable to reproduce the lowest observed flows of the lake.

The zoomed validation results for Lakes Maggiore, Como, Iseo, and Garda revealed poor model performance in reproducing both reservoir storage and outflow during the analyzed period (Mar–Jul 2016). Despite the low efficiency metrics, the model captured the overall seasonal dynamics reasonably well. In particular, the progressive increase in storage during spring followed by the early summer decline is consistently

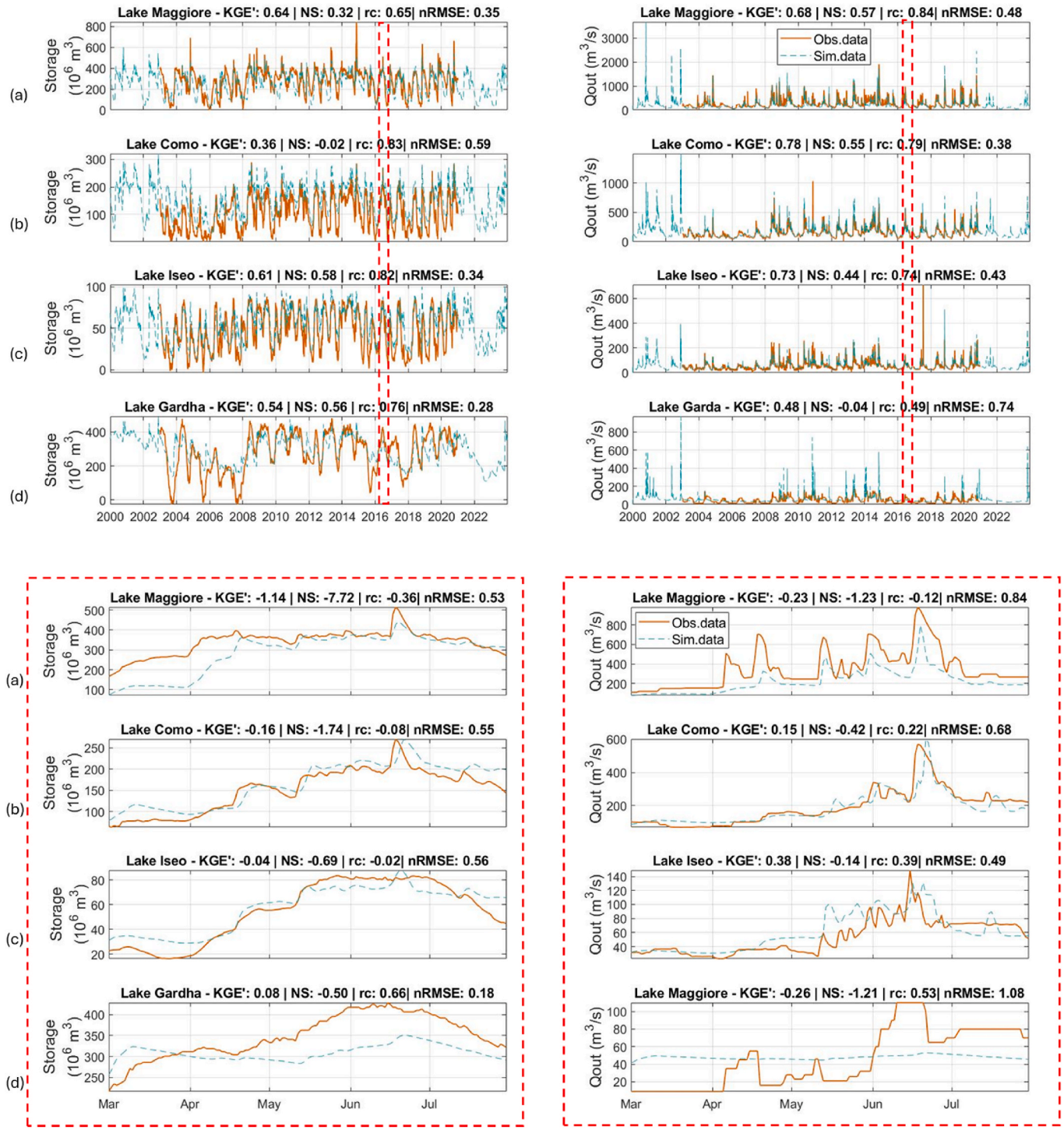

Fig. 7. Comparison between simulated and observed storage and reservoir outflows for Maggiore (plot a), Como (plot b), Iseo (plot c), and Garda (plot d) reservoirs for the time period 2000–2023. Results are zoomed for the time period Mar-Jul, 2016 in the below figure.

reproduced across the reservoirs, with nRMSE values ranging from 18% to 56% for storage. For reservoir outflows, the temporal pattern of releases is well reproduced for Lakes Maggiore, Como, and Iseo, indicating that the model captures the timing of major operational releases. However, performance metrics remained poor (nRMSE between 49% and 84%), reflecting substantial errors in discharge magnitude and peak representation. In contrast, Lake Garda showed very poor performance, with an nRMSE of 108%, and even the temporal pattern of simulated outflow did not align well with observations. Overall, considering that the investigated lakes are highly regulated, the model performance can be regarded as satisfactory for simulating reservoir storage and outflow dynamics.

6.3.3. *Irrigation modelling*

The *MISDc v3.1* model is further validated against irrigation estimates. The comparison of annual irrigation volumes derived from satellite observations, model simulations, and SIGRIAN observations across the entire basin is presented in Fig. 8a. As it can be noted, a good level of agreement is observed among the three data sources, with annual irrigation volumes ranging from approximately 10 to 14 km^3 during the

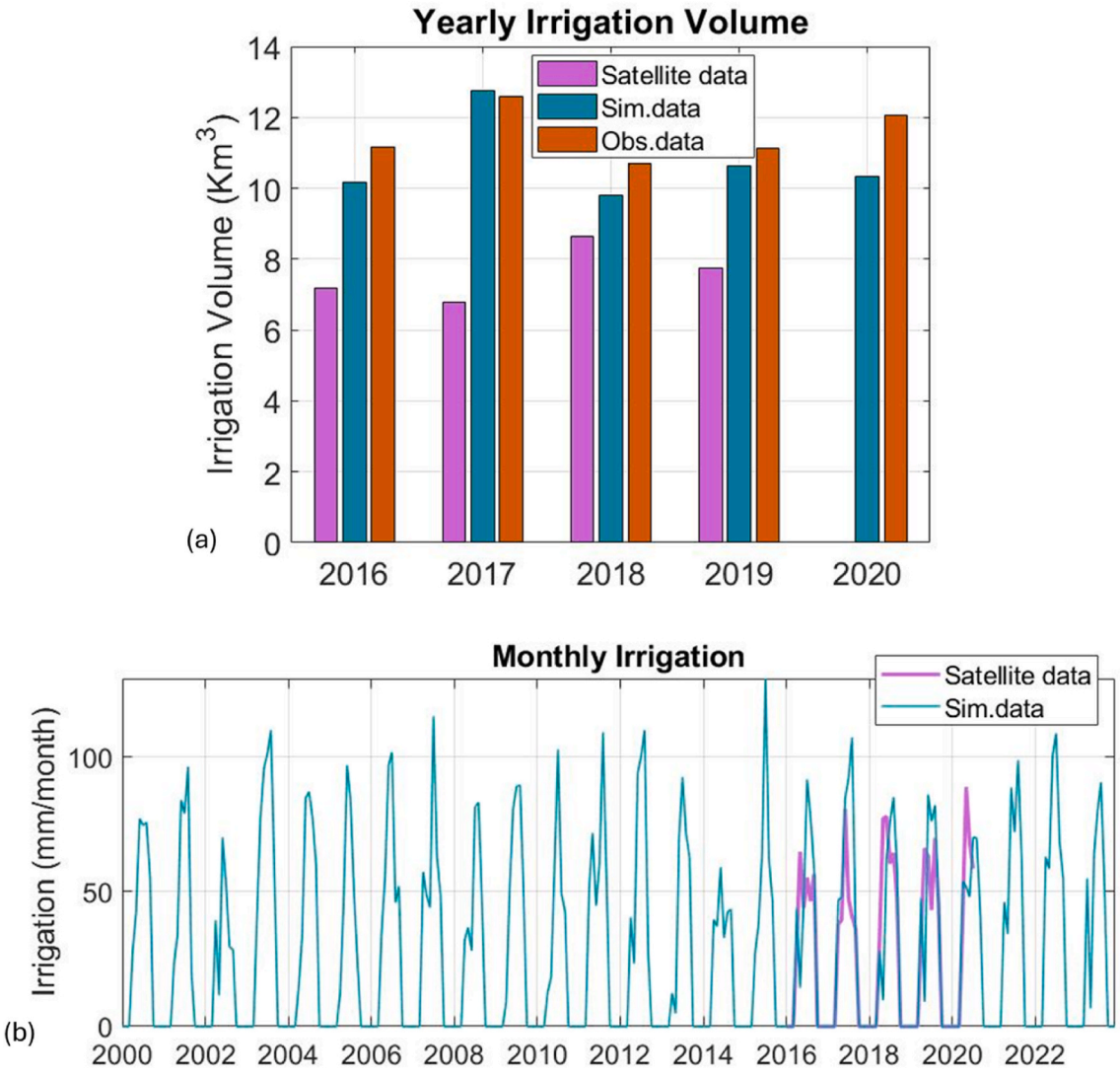

Fig. 8. Comparison between simulated (Sim.data), satellite-based, and SIGRIAN (Obs.data) irrigation estimates over the entire Po River basin at yearly (plot a) and monthly (plot b) scale from 2000 to 2023.

2016–2021 period. The model successfully reproduced the interannual variability of irrigation demand at the basin scale. Concerning the monthly analysis, evaluated at the Casale Monferrato and Cremona sections (Fig. S1e) and at the basin outlet (Pontelagoscuro, Fig. 8b), the model consistently captured the timing of irrigation onset and cessation. This demonstrated a good representation of seasonal water demand and irrigation scheduling across all three sections. The model successfully reproduced the irrigation cycle, with no applications during the winter months and progressive increases towards peak summer demand. In terms of magnitude, simulated irrigation showed higher peak values, particularly during 2016 and 2017, compared to satellite-based estimates across all three sections. However, during the period 2017–2020, the modelled and satellite-derived irrigation showed strong agreement in both seasonal patterns and peak timing, indicating improved consistency in representing irrigation variability. These results indicated that the model performed well in capturing both the seasonal dynamics and interannual variability of irrigation across the basin. While some discrepancies remained in peak irrigation magnitude, particularly in certain years, the model provided a robust representation of irrigation timing and variability, supporting its use for basin-scale water resource assessments. Concerning the seasonal analysis (2016-2021), the model exhibited lower values in certain months and higher values in others compared to satellite irrigation within the Pianura Padana region (see Fig. S2e). The analysis is not conducted in the Apennine and Alpine regions, where irrigation is almost negligible.

6.4. *Closure of the water balance*

The annual water balance closure along the Po River is presented in Fig. S3. The scatterplot of annual inflows versus outflows at Spessa, Cremona, Piancenza and Pontelagoscuro sections showed that data points closely align with the 1:1 line across all gauging stations, indicating overall consistency in mass conservation (Fig. S3a). A slightly larger dispersion is observed at higher flow volumes, but no systematic bias is evident.

The temporal evolution of annual inflow and outflow at Pontelagoscuro reveals a strong interannual coherence, with both fluxes responding consistently to wet and dry years (Fig. S3b). On average, inflow fluxes correspond to 84 $km^3\ yr^{-1}$, calculated as the sum of mean annual precipitation over the basin (74 $km^3\ yr^{-1}$) and irrigation supply (10 $km^3\ yr^{-1}$). Outflow fluxes include river discharge at the outlet (44 $km^3\ yr^{-1}$), total evaporation (39 $km^3\ yr^{-1}$, consistent with Bruno et al., 2024), and deep percolation to subsurface flows (1.5 $km^3\ yr^{-1}$). This implies an ET/P ratio of approximately 0.53, indicating that a substantial fraction of precipitation is returned to the atmosphere. Groundwater recharge (7 $km^3\ yr^{-1}$) slightly exceeds groundwater

withdrawals (6 km^3 yr^{-1}), indicating near-equilibrium aquifer conditions on an annual basis. Withdrawals consist of civil and industrial water use (4 km^3 yr^{-1}) and approximately 17% of irrigation demand (about 1.7 km^3 yr^{-1}) supplied by groundwater. The remaining irrigation demand is supplied by surface water and reservoir sources, with approximately 8 km^3 yr^{-1} withdrawn from river runoff and about 0.3 km^3 yr^{-1} from reservoirs. Overall, these estimates suggest that, at the basin scale and on an annual basis, water availability is sufficient to sustain current levels of water use.

Annual residuals, expressed as percentage deviations from total inflow, are generally contained within ±10%, with most years falling below 5% (Fig. S3c). Deviations remain moderate without persistent

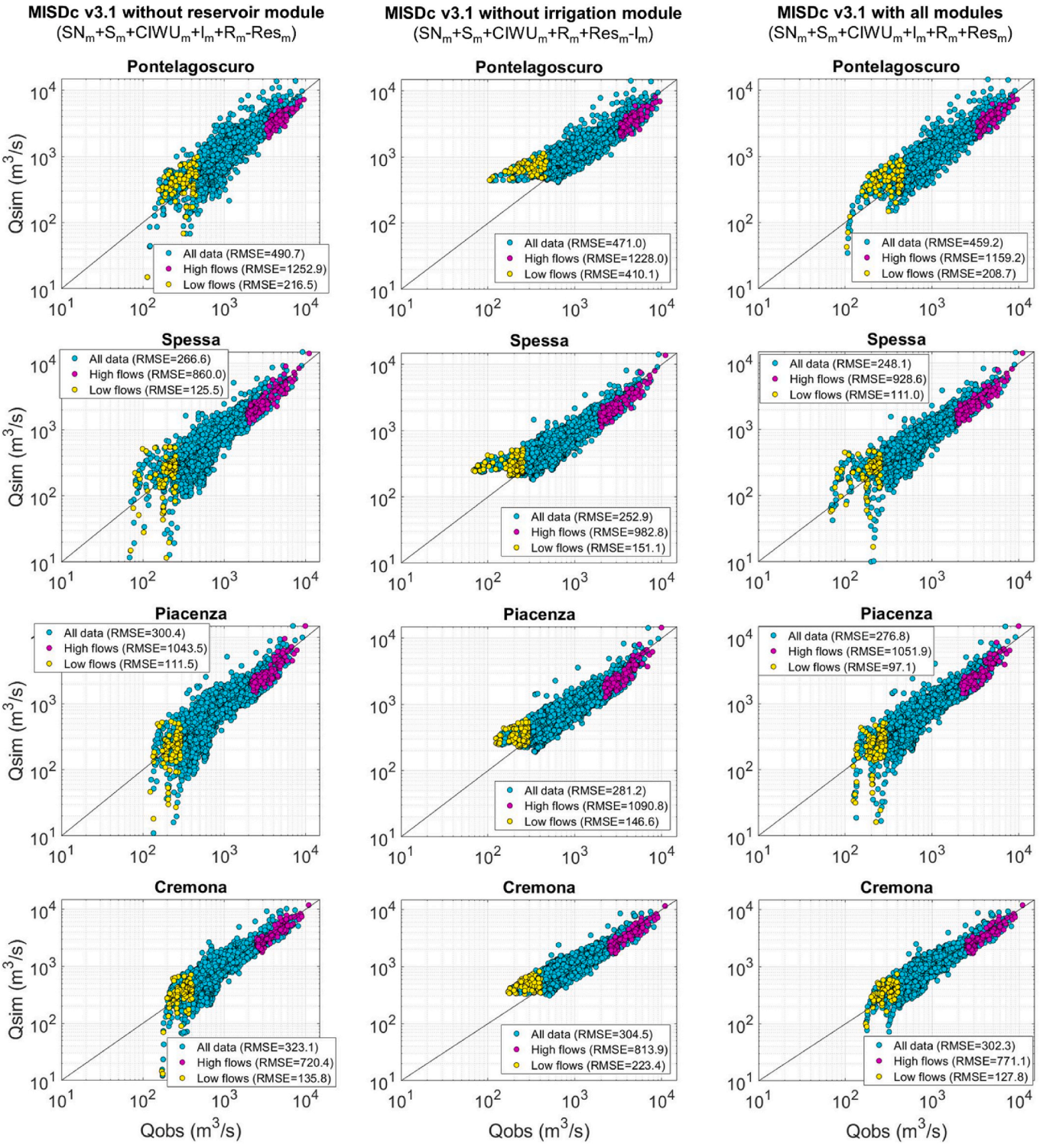

Fig. 9. Scatter plots between observed (Qobs) and simulated (Qsim) river discharge at Pontelagoscuro (calibrated), Spessa (calibrated), Cremona (uncalibrated), and Piacenza (uncalibrated) located on the main reaches of the Po River. Cyan dots refer to all river discharge values, yellow dots refer to low flow values (extracted as 5th percentile of Qobs), magenta dots refer to high flow values (extracted as 95th percentile of Qobs). (For interpretation of the references to colour in this figure legend, the reader is referred to the Web version of this article.)

over- or underestimation trends, although larger discrepancies tend to occur during hydrologically extreme years, likely reflecting increased uncertainty in flux estimation under such conditions. Overall, these results indicate satisfactory water balance closure at the basin scale. The strict 3% closure criterion (Jongen et al., 2024) is met on average over the long-term analysis, confirming the internal consistency of the modelling framework for extended simulations.

6.5. Impact of anthropogenic modules on streamflow simulation

The influence of anthropogenic modules on streamflow simulation across different flow regimes is illustrated in Fig. 9. The scatter plots compared the observed and simulated river discharge values on logarithmic scales at Pontelagoscuro, Spessa, Cremona, and Piacenza sections along the Po River and highlighted the impact of reservoir and irrigation modules on all flow regimes. Data points are categorized by flow regime, with high flows representing discharge values above the 95th percentile and low flows representing values below the 5th percentile, where percentile values are evaluated using observed river discharge values. The analysis revealed high accuracy across all sections when the complete model configuration, i.e., including the reservoir and irrigation modules, is employed. The reservoir and irrigation modules showed different impacts depending on flow conditions. For high flows, both modules have relatively minor influence, with RMSE differences of 10-100 m^3/s between the full model and configurations excluding these components which is a negligible difference given the magnitude of high flow events. In contrast, low flows exhibited greater sensitivity to both modules. The model performance improved by 3.19% at Pontelagoscuro, 11.39% at Spessa, 5.60% at Cremona, and 12.91% at Piacenza when the reservoir module was included. Similarly, including the irrigation module yielded even greater improvements of 48.89%, 26.40%, 42.61%, and 33.76%, respectively. To further isolate the contribution of irrigation, an analysis of model simulations excluding the irrigation module is conducted for both flood events (2019, 2014, and 2002; left panel, Fig. 10) and drought events (2022, 2017, and 2012; right panel, Fig. 10). The irrigation processes have a negligible effect on flood simulations, with nRMSE values remaining nearly unchanged. In contrast, the model without irrigation showed reduced performance during drought events with nRMSE of 56%–83% for 2022, 26%–35% for 2017, and 32%–59% for 2012.

7. Discussion

MISDc v3.1 represented a significant advancement in hydrological modelling by incorporating critical human water management components including reservoir operations, irrigation modelling, and water needs for civil and industrial activities alongside sophisticated representations of natural hydrological processes. The methodology integrated multiple data sources, including precipitation and air temperature records and anthropogenic water use patterns, to develop a robust modelling framework able to simulate the full spectrum of hydrological conditions and reproduce the key hydrological processes accurately.

The framework was applied to the Po River basin, a hydroclimatically heterogeneous and intensively managed system characterized by strong regulation and increasing climate variability. Despite this complexity, the *MISDc v3.1* model remained highly efficient, requiring only about 90 s to simulate the hydrological cycle over the period 2000–2023 at a daily time scale for the entire basin. The model demonstrated a better predictive accuracy at sections located on the main river compared to tributary monitoring stations. The observed performance disparities between validation sections can be attributed to the calibration strategy, wherein parameters are optimized using gauge stations positioned along the main reaches of Po River. In particular, the poor model performance at Stura di Demonte@Gaiola, Bormida@Cassine, and Taro@S.Secondo stations may be attributed to their proximity to the Alpine region, where the absence of small upstream reservoirs in the *MISDc v3.1* model together with complex topographic influences and orographic precipitation patterns, likely introduce additional hydrological processes not adequately captured by the current model parameterization. The model overestimated simulated river discharge during certain flood events (October 2000, November 2011, January 2014, November 2019). This overestimation resulted from the model's inability to account for flood peak attenuation caused by floodplain inundation, which is not currently incorporated in the *MISDc v3.1* model.

In this context, evaluating the model's ability to reproduce internal hydrological variables provided further insight into its overall performance. The model showed strong skill in capturing the seasonal and interannual dynamics of key hydrological processes by simulating soil moisture, evaporation, snow water equivalent, and irrigation. Seasonal evaluation of surface and root-zone soil moisture showed deviations from the GLEAM dataset in the Alpine region, likely because GLEAM does not explicitly account for snow accumulation and melt processes. Lower evaporation values simulated by the model compared to GLEAM across the Apennines, Alps, and Pianura Padana may be attributed to use of the modified Blaney-Criddle equation, which considers only air temperature as input. Further, incorporating a plant module would likely improve evapotranspiration estimates by explicitly representing vegetation-driven processes such as transpiration, interception, and root water uptake.

Extending this evaluation to regulated water bodies further highlighted the challenges associated with representing human-controlled hydrological processes. A better model performance in simulating Lake Como outflow despite poor storage simulation highlighted the complex relationship between storage volume and regulated releases. The poor model performance in simulating storage may be attributed to the dual operation of Lake Como as both a storage system and a run-of-the-river hydropower facility, where water levels are managed within constrained operating ranges and influenced by hydropower requirements not explicitly represented in the current model. The model failed to capture the storage drawdowns of Lake Garda, which likely correspond to drought periods when special management interventions are implemented. The poor performance of the model in simulating the outflow of Lake Garda reflected the highly managed nature of this lake, where outflows are regulated according to specific operational rules rather than following a simple storage-discharge relationship. In particular, Lake Garda operates also as a mixed pumped-storage hydropower system (Galletti et al., 2025), which is not represented in the current model version and may contribute to the observed discrepancies. The complexity of simulating Lake Garda is explained by Hinegk et al. (2022), who analyzed 133 years (1888-2020) of water levels and outflow data, demonstrating that regulation since 1951 has created complex management scenarios that exceed standard modelling capabilities. The model performance in simulating the storage dynamics and reservoir outflows can be improved by considering the hydropower requirements.

Beyond reservoir regulation, evaluating irrigation processes provided additional insight into the model's representation of anthropogenic water use across the basin. The seasonal analysis of irrigation revealed lower agreement with satellite-based estimates across the Pianura Padana region. This discrepancy is likely related to the use of SIGRIAN information to define irrigated areas rather than satellite-derived irrigation dataset. Consequently, while the model performed well at the basin scale, regional seasonal analyses highlighted limitations in representing the spatial and temporal distribution of irrigation. The model also showed strong performance in simulating civil and industrial water use at the aggregated scale, as validation against water demand data from the Po River Basin Authority demonstrated that the model closely reproduced the reported annual supply for civil and industrial activities (~4 $km^3\ yr^{-1}$), confirming its robustness in representing basin-scale anthropogenic water demand. Furthermore, the

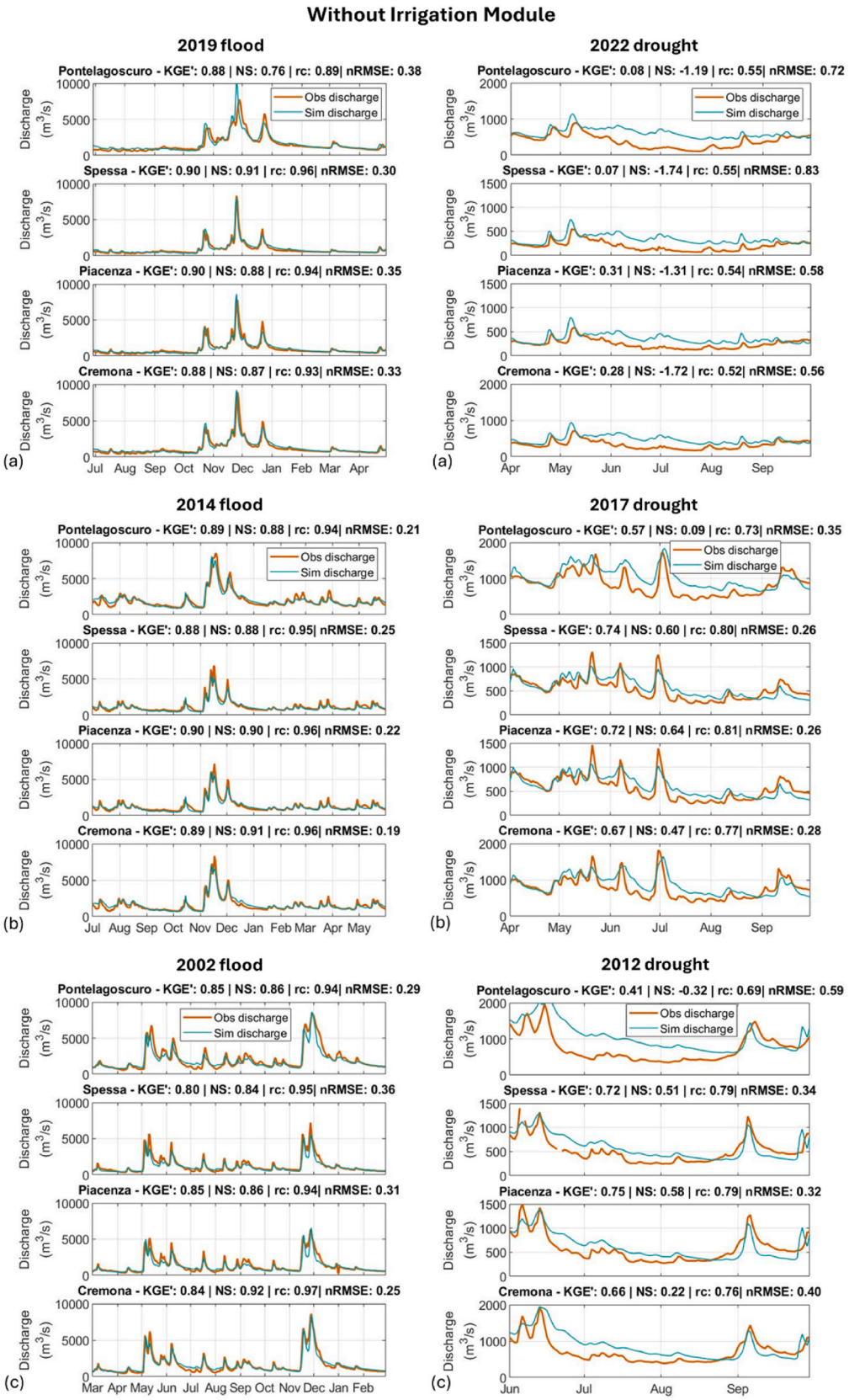

Fig. 10. Extreme hydrological events without irrigation module at Pontelagoscuro (calibrated), Spessa (calibrated), Piacenza (uncalibrated) and Cremona (uncalibrated) sections located on the main reaches of the Po River. The left Panels illustrate flood events in 2019 (plot a), 2014 (plot b), and 2002 (plot c), while the right panels show drought events in 2022 (plot a), 2017 (plot b) and 2012 (plot c).

strong agreement between annual inflows and outflows, with residuals generally below ±10% (and under 5% in most years), supports the robustness of the model in maintaining basin-scale mass conservation.

Within this broader framework of anthropogenic water management, the analysis of the impact of anthropogenic modules on streamflow conditions highlighted the dominant role of irrigation withdrawals in controlling low-flow dynamics. This is reflected in the substantially larger performance improvements observed when the irrigation module is included compared to reservoir operations. This behaviour is likely related to the representation of only major regulated reservoirs in the model, while smaller reservoirs and hydropower-dominated alpine systems are not included, which is particularly important given that hydropower regulation plays a key role in shaping sub-monthly inflow patterns in major Italian lakes and in controlling short-term responses to both flood and drought conditions. The incorporation of the irrigation module enhanced simulated flow accuracy during major drought events, achieving performance improvements of 8% - 42.2%, 1.3% - 24.2%, and 11.3% - 30,6% for the 2022, 2017, and 2012 droughts, respectively. Overall, these results demonstrated that incorporating both reservoir and irrigation modules significantly improves model performance across all flow regimes, with particularly notable benefits for low flow simulation where anthropogenic water management practices play a dominant role.

8. Conclusions

This study introduced the *MISDc v3.1* hydrological model and comprehensively evaluated its capability to simulate the complex water dynamics of the Po River Basin across multiple hydrological components. Its reduced structural complexity translates into very low computational demand, enhancing both flexibility and scalability. Specifically, the model is well suited for: (1) testing alternative input and output datasets for calibration and validation, including satellite-based observations; and (2) exploring "what-if" scenarios that require thousands of model realizations under varying configurations. Owing to its flexibility, modular structure, and computational efficiency, *MISDc v3.1* is therefore particularly suitable for integration into digital twin frameworks of the water cycle. The following key findings demonstrated that *MISDc v3.1* provides a valuable framework for integrated water resources management in large, complex river systems, while identifying specific areas to focus on in future studies to achieve more comprehensive hydrological process representation.

- The performance disparities between validation sections indicates the necessity of calibration on tributaries as well, to better capture the localized hydrological processes, flow generation mechanisms, and sub-basin characteristics, thereby improving the overall representation of basin-wide hydrological processes (see Table 3).
- The model shows robust performance during extreme hydrological conditions (see Fig. 4).
- Uncertainty assessment for the river discharge simulation provides valuable additional information for end users, allowing them to quantify reliability of the prediction across the whole range of river flow.
- The model performance against other hydrological processes can be further enhanced by multi-variable calibration using observational datasets (Fig. 6).
- Model performance in simulating the storage dynamics and reservoir outflows of Lakes Garda can be improved by considering the hydropower requirements (See Fig. 7).
- Satellite observations are very useful to assess model performance for the different storages (soil moisture and snow), fluxes (evaporation) and human impact (irrigation).
- Incorporating a plant module would likely improve evapotranspiration estimates by explicitly representing vegetation-driven processes such as transpiration, interception, and root water uptake.
- The Irrigation module has a more pronounced impact on low-flow simulation than reservoir operations, mainly because the current model does not account for smaller reservoirs and hydropower-dominated Alpine systems (see Fig. 9).
- Including the irrigation and reservoir modules significantly improves river discharge, particularly for low flows (see Fig. 9).
- Model performance of low flows can be improved by including hydropower-dominated Alpine systems in the model, which is particularly important given that hydropower regulation plays a key role in shaping sub-monthly inflow patterns in major Italian lakes and in controlling short-term responses to both flood and drought conditions.
- Model accuracy during low-flow periods can be further improved by the acquisition of high-precision ground truth irrigation data.

Furthermore, the *MISDc v3.1* modelling framework is highly replicable and easily transferable for other sub-basins. The model's Python codebase is available through open-access repositories, facilitating easy modification and adaptation for diverse hydrological applications.

Software section

The *MISDc v3.1* model code is available online at https://github.com/sindhu-kalimisetty/MISDc-v3.1-Hydrological-Model (python version). along with detailed documentation for application installation, testing, and deployment.

BLUECAT is available at: https://github.com/albertomontanari/Bluecat-R and https://github.com/albertomontanari/Bluecat-Python (R and Python versions, respectively), along with detailed documentation for application installation, testing, and deployment. Further information is provided by the R help (included in the R version)

CRediT authorship contribution statement

Sindhu Kalimisetty: Data curation, Formal analysis, Investigation, Methodology, Software, Validation, Visualization, Writing – original draft. **Alberto Montanari:** Conceptualization, Formal analysis, Funding acquisition, Investigation, Writing – review & editing. **Serena Ceola:** Formal analysis, Funding acquisition, Investigation, Writing – review & editing. **Irene Palazzoli:** Formal analysis, Investigation, Writing – review & editing. **Paolo Stocchi:** Writing – review & editing. **Paolo Filippucci:** Software, Writing – review & editing. **Luca Brocca:** Conceptualization, Writing – review & editing. **Jacopo Dari:** Writing – review & editing. **Francesco Tornatore:** Writing – review & editing. **Federica Bonaiuti:** Writing – review & editing. **Stefania Camici:** Data curation, Formal analysis, Funding acquisition, Investigation, Methodology, Project administration, Software, Supervision, Validation, Visualization, Writing – review & editing.

Declaration of competing interest

The authors declare the following financial interests/personal relationships which may be considered as potential competing interests: Stefania Camici reports financial support was provided by Ministry of University and Research Italy. Alberto Montanari reports financial support was provided by Ministry of University and Research Italy. Alberto Montanari reports financial support was provided by Italian Science Fund. If there are other authors, they declare that they have no known competing financial interests or personal relationships that could have appeared to influence the work reported in this paper.

Acknowledgments

The authors gratefully acknowledge support from MUR. Alberto Montanari and Serena Ceola were supported by the RETURN Extended Partnership which received funding from the European Union Next-

GenerationEU (National Recovery and Resilience Plan – NRRP, Mission 4, Component 2, Investment 1.3 – D.D. 1243 2/8/2022, PE0000005). Alberto Montanari was also supported by the Italian Science Fund through the project "Stochastic amplification of climate change into floods and droughts change ($CO_2$2Water)", grant number J53C23003860001. Stefania Camici, Serena Ceola, Irene Palazzoli were supported by the "unveilINg pasT Events foR dROught risk mitiGATION (INTERROGATION) project funded by the MUR Progetti di Ricerca di Rilevante Interesse Nazionale (PRIN) Bando 2022 - grant 202295TM87.

Appendix A. Supplementary data

Supplementary data to this article can be found online at https://doi.org/10.1016/j.envsoft.2026.107056.

Data availability

Data will be made available on request.

References

Abdelkader, M., Temimi, M., Ouarda, T.B.M.J., 2023. Assessing the national water model's streamflow estimates using a multi-decade retrospective dataset across the contiguous United States. Water (Switzerland) 15. https://doi.org/10.3390/w15132319.

AghaKouchak, A., Mirchi, A., Madani, K., Di Baldassarre, G., Nazemi, A., Alborzi, A., et al., 2021. Anthropogenic Drought: Definition, Challenges, and Opportunities.

Alfieri, L., Avanzi, F., Delogu, F., Gabellani, S., Bruno, G., Campo, L., et al., 2021. High resolution satellite products improve hydrological modeling in northern Italy. Hydrol. Earth Syst. Sci. Discuss. 2021, 1–29.

Astagneau, P.C., Thirel, G., Delaigue, O., Guillaume, J.H., Parajka, J., Brauer, C.C., et al., 2021. Hydrology modelling R packages–a unified analysis of models and practicalities from a user perspective. Hydrol. Earth Syst. Sci. 25 (7), 3937–3973.

Avanzi, F., Gabellani, S., Delogu, F., Silvestro, F., Cremonese, E., Morra di Cella, U., Ratto, S., Stevenin, H., 2022. Snow multidata Mapping and Modeling (S3M) 5.1: a distributed cryospheric model with dry and wet snow, data assimilation, glacier mass balance, and debris-driven melt. Geosci. Model Dev. 15, 4853–4879. https://doi.org/10.5194/gmd-15-4853-2022.

Avanzi, F., Munerol, F., Milelli, M., Gabellani, S., Massari, C., Girotto, M., et al., 2024. Winter snow deficit was a harbinger of summer 2022 socio-hydrologic drought in the Po Basin, Italy. Commun. Earth Environ. 5 (1), 64.

Berselli, M., 2022. Acque Sotterranee, Giacimento Della Risorsa Idrica. Autorità Di Bacino Distrettuale Del Fiume Po. chrome-extension://efaidnbmnnnibpcajpcglclefindmkaj. https://www.adbpo.it/wp-content/uploads/2022/03/Presentazione_Berselli_acque-sotterranee_220322.pdf.

Beven, K., 2006. A manifesto for the equifinality thesis. Journal of hydrology 320 (1–2), 18–36.

Beven, K., Binley, A., 2014. GLUE: 20 years on. Hydrol. Process. 28 (24), 5897–5918.

Beven, K.J., Chappell, N.A., 2021. Perceptual perplexity and parameter parsimony. Wiley Interdiscip. Rev.: Water 8 (4), e1530.

Bozzola, M., Swanson, T., 2014. Policy implications of climate variability on agriculture: water management in the po river basin, Italy. Environ. Sci. Pol. 43, 26–38.

Brocca, L., Barbetta, S., Camici, S., Ciabatta, L., Dari, J., Filippucci, P., Massari, C., Modanesi, S., Tarpanelli, A., Bonaccorsi, B., Mosaffa, H., Wagner, W., Vreugdenhil, M., Quast, R., Alfieri, L., Gabellani, S., Avanzi, F., Rains, D., Miralles, D. G., Mantovani, S., Briese, C., Domeneghetti, A., Jacob, A., Castelli, M., Camps-Valls, G., Volden, E., Fernandez, D., 2024. A digital twin of the terrestrial water cycle: a glimpse into the future through high-resolution Earth observations. Front. Sci. 1. https://doi.org/10.3389/fsci.2023.1190191.

Brocca, L., Liersch, S., Melone, F., Moramarco, T., Volk, M., 2013. Application of a model-based rainfall-runoff database as efficient tool for flood risk management. Hydrol. Earth Syst. Sci. 17, 3159–3169. https://doi.org/10.5194/hess-17-3159-2013.

Brocca, L., Massari, C., Pellarin, T., Filippucci, P., Ciabatta, L., Camici, S., Kerr, Y.H., Fernández-Prieto, D., 2020. River flow prediction in data scarce regions: soil moisture integrated satellite rainfall products outperform rain gauge observations in West Africa. Sci. Rep. 10, 12517. https://doi.org/10.1038/s41598-020-69343-x.

Brocca, L., Melone, F., Moramarco, T., 2011. Distributed rainfall-runoff modelling for flood frequency estimation and flood forecasting. Hydrol. Process. 25 (18), 2801–2813.

Brunetti, M., Lentini, G., Maugeri, M., Nanni, T., Simolo, C., Spinoni, J., 2012. Projecting north eastern Italy temperature and precipitation secular records onto a high-resolution grid. Physics and Chemistry of the Earth, Parts A/B/C, 40–41 9–22. https://doi.org/10.1016/j.pce.2009.12.005.

Bruno, G., Avanzi, F., Alfieri, L., Libertino, A., Gabellani, S., Duethmann, D., 2024. Hydrological model skills change with drought severity; insights from multi-variable evaluation. J. Hydrol. 634, 131023.

Burek, P., Satoh, Y., Kahil, T., Tang, T., Greve, P., Smilovic, M., et al., 2020. Development of the community water model (CWatM v1. 04)–a high-resolution hydrological model for global and regional assessment of integrated water resources management. Geosci. Model Dev. 13 (7), 3267–3298.

Camici, S., Brocca, L., Melone, F., Moramarco, T., 2014. Impact of climate change on flood frequency using different climate models and downscaling approaches. J. Hydrol. Eng. 19. https://doi.org/10.1061/(ASCE)HE.1943-5584.0000959.

Camici, S., Ciabatta, L., Massari, C., Brocca, L., 2018. How reliable are satellite precipitation estimates for driving hydrological models: a verification study over the mediterranean area. J. Hydrol. (Amst.) 563, 950–961. https://doi.org/10.1016/j.jhydrol.2018.06.067.

Camici, S., Dari, J., Filippucci, P., Massari, C., Mantovani, S., Avanzi, F., et al., 2025. High-resolution satellite observations for developing advanced decision support systems for water resources management in the Po River. J. Hydrol., 134047

Camici, S., Giuliani, G., Brocca, L., Massari, C., Tarpanelli, A., Farahani, H.H., Sneeuw, N., Restano, M., Benveniste, J., 2022. Synergy between satellite observations of soil moisture and water storage anomalies for runoff estimation. Geosci. Model Dev. 15, 6935–6956. https://doi.org/10.5194/gmd-15-6935-2022.

Camici, S., Massari, C., Ciabatta, L., Marchesini, I., Brocca, L., 2020. Which rainfall score is more informative about the performance in river discharge simulation? A comprehensive assessment on 1318 basins over Europe. Hydrol. Earth Syst. Sci. 24, 4869–4885. https://doi.org/10.5194/hess-24-4869-2020.

Carminati, E., Martinelli, G., 2002. Subsidence rates in the Po Plain, northern Italy: the relative impact of natural and anthropogenic causation. Eng. Geol. 66 (3–4), 241–255. https://doi.org/10.1016/S0013-7952(02)00031-5.

Castellarin, A., Di Baldassarre, G., Brath, A., 2011. Floodplain management strategies for flood attenuation in the river Po. River Res. Appl. 27 (8), 1037–1047.

Cavalleri, F., Viterbo, F., Brunetti, M., Bonanno, R., Manara, V., Lussana, C., Lacavalla, M., Maugeri, M., 2024. Inter-comparison and validation of high-resolution surface air temperature reanalysis fields over Italy. Int. J. Climatol. 44, 2681–2700. https://doi.org/10.1002/joc.8475.

Cislaghi, A., Masseroni, D., Massari, C., Camici, S., Brocca, L., 2020. Combining a rainfall–runoff model and a regionalization approach for flood and water resource assessment in the western Po Valley, Italy. Hydrol. Sci. J. 65, 348–370. https://doi.org/10.1080/02626667.2019.1690656.

Dari, J., Brocca, L., Modanesi, S., Massari, C., Tarpanelli, A., Barbetta, S., Quast, R., Vreugdenhil, M., Freeman, V., Barella-Ortiz, A., Quintana-Seguí, P., Bretreger, D., Volden, E., 2023. Regional data sets of high-resolution (1 and 6 km) irrigation estimates from space. Earth Syst. Sci. Data 15, 1555–1575. https://doi.org/10.5194/essd-15-1555-2023.

De Lannoy, G.J.M., Bechtold, M., Busschaert, L., Heyvaert, Z., Modanesi, S., Dunmire, D., Lievens, H., Getirana, A., Massari, C., 2024. Contributions of irrigation modeling, soil moisture and snow data assimilation to high-resolution water budget estimates over the Po Basin: progress towards digital Replicas. J. Adv. Model. Earth Syst. 16 (10). https://doi.org/10.1029/2024MS004433.

De Lavenne, A., Andréassian, V., Thirel, G., Ramos, M.H., Perrin, C., 2019. A regularization approach to improve the sequential calibration of a semidistributed hydrological model. Water Resour. Res. 55 (11), 8821–8839.

De Santis, D., Biondi, D., Crow, W.T., Camici, S., Modanesi, S., Brocca, L., Massari, C., 2021. Assimilation of satellite soil moisture products for river flow prediction: an extensive experiment in over 700 catchments throughout Europe. Water Resour. Res. 57. https://doi.org/10.1029/2021WR029643.

Ding, Z., Lü, H., Ahmed, N., Zhu, Y., Gou, Q., Wang, X., Liu, E., Xu, H., Pan, Y., Sun, M., 2022. Soil moisture data assimilation in MISDc for improved hydrological simulation in upper Huai River Basin, China. Water 14 (21), 3476. https://doi.org/10.3390/w14213476.

Doorenbos, J., Pruitt, W.O., 1977. Background and development of methods to predict reference crop evapotranspiration (ETo). Appendix II in FAO-ID- 24, 108–119.

Droppers, B., Franssen, W.H.P., van Vliet, M.T.H., Nijssen, B., Ludwig, F., 2020. Simulating human impacts on global water resources using VIC-5. Geosci. Model Dev. 13 (10), 5029–5052. https://doi.org/10.5194/gmd-13-5029-2020.

Evangelista, G., Mazzoglio, P., Ganora, D., Pianigiani, F., Claps, P., 2025. Features of Italian large dams and their upstream catchments. Earth Syst. Sci. Data 17, 1407–1426. https://doi.org/10.5194/essd-17-1407-2025.

Formetta, G., Tootle, G., Therrell, M., 2022. Regional reconstruction of Po River Basin (Italy) streamflow. Hydrology 9. https://doi.org/10.3390/hydrology9100163.

Galelli, S., Turner, S.W., Pokhrel, Y., Yi Ng, J., Castelletti, A., Bierkens, M.F., et al., 2025. Advancing the representation of human actions in large-scale hydrological models: challenges and future research directions. Water Resour. Res. 61 (7) e2024WR039486.

Galletti, A., Zarghami Dastjerdi, S., Majone, B., 2025. Comprehensive inventory of large hydropower systems in the Italian Alpine Region. Earth Syst. Sci. Data 17, 3353–3373. https://doi.org/10.5194/essd-17-3353-2025.

Georgakakos, K.P., Baumer, O.W., 1996. Measurement and utilization of on-site soil moisture data. J. Hydrol. 184 (1–2), 131–152. https://doi.org/10.1016/0022-1694(95)02971-0.

GRDC, 2020. GRDC Major River Basins. Global Runoff Data Centre. 2nd, Rev. Ed. Koblenz: Federal Institute of Hydrology (Bfg).

Han, M., Shen, H., Tolson, B.A., Craig, J.R., Mai, J., Lin, S.G., et al., 2023. BasinMaker 3.0: a GIS toolbox for distributed watershed delineation of complex lake-river routing networks. Environ. Model. Software 164, 105688.

Hernandez-Samaniego, E., Navarro-Gomez, C., Sánchez, D.H., Sánchez-Navarro, J.R., 2023. Coefficients and curves of hourly and daily variations of water demand for improved operation of potable water distribution systems: a case study of Chihuahua City, Mexico. Water Pract. Technol. 18 (8), 1991–2001. https://doi.org/10.2166/wpt.2023.117.

Hinegk, L., Adami, L., Zolezzi, G., Tubino, M., 2022. Implications of water resources management on the long-term regime of Garda lake (Italy). J. Environ. Manag. 301, 113893. https://doi.org/10.1016/j.jenvman.2021.113893.
Hu, G.R., Li, X.Y., 2018. Subsurface flow. In: Li, X., Vereecken, H. (Eds.), Observation and Measurement, Ecohydrology. Springer, Berlin, Heidelberg.
Jongen, H.J., Lipson, M., Teuling, A.J., Grimmond, S., Baik, J.J., Best, M., et al., 2024. The water balance representation in urban-PLUMBER land surface models. J. Adv. Model. Earth Syst. 16 (10) e2024MS004231.
Kebede, E.A., Oluoch, K.O.A., Siebert, S., Mehta, P., Hartman, S., Jägermeyr, J., et al., 2025. A global open-source dataset of monthly irrigated and rainfed cropped areas (MIRCA-OS) for the 21st century. Sci. Data 12 (1), 208.
Klabunde, A., Kapoor, S., Franceschini, A., Paye-Layleh, L., Aldaria, A., Kauffman, G., 2025. REPORT Remediation for the Environment of the Po River Territory: Regional Watershed Management.
Kling, H., Fuchs, M., Paulin, M., 2012. Runoff conditions in the upper Danube basin under an ensemble of climate change scenarios. J. Hydrol. (Amst.) 424–425, 264–277. https://doi.org/10.1016/j.jhydrol.2012.01.011.
Knoben, W.J.M., Freer, J.E., Woods, R.A., 2019. Technical note: inherent benchmark or not? Comparing Nash-Sutcliffe and Kling-Gupta efficiency scores (preprint). Catchment hydrology/modelling Approaches.
Koutsoyiannis, D., Montanari, A., 2022. Bluecat: a local uncertainty estima-tor for deterministic simulations and predictions. Water Resour. Res. 58 (1). https://doi.org/10.1029/2021WR031215 e2021WR031215.
Lehner, B., Liermann, C.R., Revenga, C., Vörösmarty, C., Fekete, B., Crouzet, P., et al., 2011. High-resolution mapping of the world's reservoirs and dams for sustainable river-flow management. Front. Ecol. Environ. 9 (9), 494–502.
Li, H., Xu, C.Y., Beldring, S., 2015. How much can we gain with increasing model complexity with the same model concepts? J. Hydrol. 527, 858–871.
Liu, J., Yang, H., Gosling, S.N., Kummu, M., Flörke, M., Pfister, S., Hanasaki, N., Wada, Y., Zhang, X., Zheng, C., Alcamo, J., Oki, T., 2017. Water scarcity assessments in the past, present, and future. Earths Future 5, 545–559. https://doi.org/10.1002/2016EF000518.
Maidment, D.R., Miaou, S.-P., 1986. Daily water use in nine cities. Water Resour. Res. 22 (6), 845–851. https://doi.org/10.1029/WR022i006p00845.
Martens, B., Miralles, D.G., Lievens, H., Van Der Schalie, R., De Jeu, R.A., Fernández-Prieto, D., et al., 2017. GLEAM v3: satellite-based land evaporation and root-zone soil moisture. Geosci. Model Dev. 10 (5), 1903–1925.
Martinec, J., 1960. The degree-day factor for snowmelt runoff forecasting. In: Proceedings of General Assembly of Helsinki Commission on Surface Waters, vol. 51. International Association of Hydrological Sciences, IAHS Publ, Wallingford, UK, pp. 468–477.
Massari, C., Brocca, L., Tarpanelli, A., Moramarco, T., 2015. Data assimilation of satellite soil moisture into rainfall-runoff modelling: a complex recipe? Remote Sens. 7 (9), 11403–11433. https://doi.org/10.3390/rs70911403.
Massari, C., Camici, S., Ciabatta, L., Brocca, L., 2018. Exploiting satellite-based surface soil moisture for flood forecasting in the mediterranean area: state update versus rainfall correction. Remote Sens. 10 (2), 292.
Masseroni, D., Cislaghi, A., Camici, S., Massari, C., Brocca, L., 2017. A reliable rainfall-runoff model for flood forecasting: review and application to a semiurbanized watershed at high flood risk in Italy. Hydrol. Res. 48 (3), 726–740. https://doi.org/10.2166/nh.2016.037.
Mazzoglio, P., Lompi, M., Marra, F., Dallan, E., Deidda, R., Claps, P., Manfreda, S., Noto, L.V., Viglione, A., Raffa, M., Mercogliano, P., Marani, M., Caporali, E., Borga, M., 2025. Orographic and land-sea contrast effects in convection-permitting simulations of extreme sub-daily precipitation. Weather Clim. Extrem. 49, 100798. https://doi.org/10.1016/j.wace.2025.100798.
Merz, R., Miniussi, A., Basso, S., Petersen, K.J., Tarasova, L., 2022. More complex is not necessarily better in large-scale hydrological modeling: a model complexity experiment across the contiguous United States. Bull. Am. Meteorol. Soc. 103 (8), E1947–E1967.
Milly, P.C.D., Betancourt, J., Falkenmark, M., Hirsch, R.M., Kundzewicz, Z.W., Lettenmaier, D.P., Stouffer, R.J., 2008. Stationarity is dead: whither water management? Science (1979) 319, 573–574. https://doi.org/10.1126/science.1151915.
Miralles, D.G., Holmes, T.R.H., De Jeu, R.A.M., Gash, J.H., Meesters, A.G.C.A., Dolman, A.J., 2011. Global land-surface evaporation estimated from satellite-based observations. Hydrol. Earth Syst. Sci. 15, 453–469. https://doi.org/10.5194/hess-15-453-2011.
Mitchell, T.D., Jones, P.D., 2005. An improved method of constructing a database of monthly climate observations and associated high-resolution grids. Int. J. Climatol. 25 (6), 693–712. https://doi.org/10.1002/joc.1181.
Montanari, A., Nguyen, H., Rubinetti, S., Ceola, S., Galelli, S., Rubino, A., Zanchettin, D., 2023. Why the 2022 po river drought is the worst in the past two centuries. Sci. Adv. 9. https://doi.org/10.1126/sciadv.adg8304.
Montanari, A., Koutsoyiannis, D., 2025. Uncertainty estimation for environmental multimodel predictions: the BLUECAT approach and software. Environ. Model. Software 188, 106419. https://doi.org/10.1016/j.envsoft.2025.106419.
Musolino, D., de Carli, A., Massarutto, A., 2017. Evaluation of socio-economic impact of drought events: the case of Po river basin. Eur. Countrys. 9, 163–176. https://doi.org/10.1515/euco-2017-0010.
Musolino, D., Vezzani, C., Massarutto, A., 2018. Drought management in the Po River Basin, Italy. In: Drought. Wiley, pp. 201–215. https://doi.org/10.1002/9781119017073.ch11.
Nash, J.E., Sutcliffe, J.V., 1970. River flow forecasting through conceptual models part I — a discussion of principles. J. Hydrol. (Amst.) 10, 282–290. https://doi.org/10.1016/0022-1694(70)90255-6.
Orth, R., Staudinger, M., Seneviratne, S.I., Seibert, J., Zappa, M., 2015. Does model performance improve with complexity? A case study with three hydrological models. J. Hydrol. 523, 147–159.
Pavan, V., Antolini, G., Barbiero, R., Berni, N., Brunier, F., Cacciamani, C., Cagnati, A., Cazzuli, O., Cicogna, A., De Luigi, C., Di Carlo, E., Francioni, M., Maraldo, L., Marigo, G., Micheletti, S., Onorato, L., Panettieri, E., Pellegrini, U., Pelosini, R., Piccinini, D., Ratto, S., Ronchi, C., Rusca, L., Sofia, S., Stelluti, M., Tomozeiu, R., Torrigiani Malaspina, T., 2019. High resolution climate precipitation analysis for north-central Italy, 1961–2015. Clim. Dyn. 52, 3435–3453. https://doi.org/10.1007/s00382-018-4337-6.
PdgP, 2010. Piano Di Gestione Del Distretto Idrografico Del Fiume Po. Autorità di bacino del Fiume Po, pp. 1–591. https://www.adbpo.it/download/PdGPo_24febbraio2010/PDGPo_ELABORATO_01_CaratteristicheDistretto/PdG_Po_ELABORATO_1_10_03_11.pdf.
PdgP, 2016. Piano di gestione del distretto idrografico del fiume Po. Autorità di bacino del Fiume Po. Allegato 1 alla Relazione Generale, Bilancio Idrico dell'asta del Fiume Po 1–87. https://www.adbpo.it/PBI/PBI_progetto_piano/02_Allegato1_Bilancio_Asta_Po_V06_10_2016.pdf.
Pearson, K., 1895. VII. Note on regression and inheritance in the case of two parents. Proc. Roy. Soc. Lond. 58, 240–242. https://doi.org/10.1098/rspl.1895.0041.
Rameshwaran, P., Bell, V.A., Brown, M.J., Davies, H.N., Kay, A.L., Rudd, A.C., Sefton, C., 2022. Use of abstraction and discharge data to improve the performance of a national-scale hydrological model. Water Resour. Res. 58 (1). https://doi.org/10.1029/2021WR029787.
Rivera, J.A., Infanti, J.M., Kumar, R., Mutemi, J.N., 2021. Editorial: challenges of hydrological drought monitoring and prediction. Front. Water 3. https://doi.org/10.3389/frwa.2021.750311.
Siebert, S., Kummu, M., Porkka, M., Döll, P., Ramankutty, N., Scanlon, B.R., 2015. A global data set of the extent of irrigated land from 1900 to 2005. Hydrol. Earth Syst. Sci. 19 (3), 1521–1545.
Singh, V.P., 2018. Hydrologic modeling: progress and future directions. Geoscience letters 5 (1), 1–18.
Telteu, C.E., Müller Schmied, H., Thiery, W., Leng, G., Burek, P., Liu, X., et al., 2021. Understanding each other's models: an introduction and a standard representation of 16 global water models to support intercomparison, improvement, and communication. Geosci. Model Dev. 14 (6), 3843–3878.
Tramblay, Y., El Khalki, E.M., Ciabatta, L., Camici, S., Hanich, L., Saidi, M.E.M., Ezzahouani, A., Benaabidate, L., Mahé, G., Brocca, L., 2023. River runoff estimation with satellite rainfall in Morocco. Hydrol. Sci. J. 68, 474–487. https://doi.org/10.1080/02626667.2023.2171295.
Veldkamp, T.I.E., Zhao, F., Ward, P.J., De Moel, H., Aerts, J.C., Schmied, H.M., et al., 2018. Human impact parameterizations in global hydrological models improve estimates of monthly discharges and hydrological extremes: a multi-model validation study. Environ. Res. Lett. 13 (5), 055008.
Vezzoli, R., Mercogliano, P., Pecora, S., Zollo, A.L., Cacciamani, C., 2015. Hydrological simulation of po river (North Italy) discharge under climate change scenarios using the RCM COSMO-CLM. Sci. Total Environ. 521–522. https://doi.org/10.1016/j.scitotenv.2015.03.096.
Wada, Y., Bierkens, M.F., De Roo, A., Dirmeyer, P.A., Famiglietti, J.S., Hanasaki, N., et al., 2017. Human–water interface in hydrological modelling: current status and future directions. Hydrol. Earth Syst. Sci. 21 (8), 4169–4193.
Wada, Y., Wisser, D., Bierkens, M.F.P., 2013. Global modeling of withdrawal, allocation and consumptive use of surface water and groundwater resources. https://doi.org/10.5194/esdd-4-355-2013.
Wang, Y., Wang, Y., Wang, Y., Li, C., Ju, Q., Jin, J., Deng, X., Sun, G., Bao, Z., 2023. Applicability of the HBV model to a human-influenced catchment in northern China. Hydrol. Res. 54 (2), 208–219. https://doi.org/10.2166/nh.2023.092.
Williams, G.P., 2025. Friends don't let friends use nash-sutcliffe efficiency (NSE) or KGE for hydrologic model accuracy evaluation: a rant with data and suggestions for better practice. Environ. Model. Software, 106665.
Zhang, Y., Wu, Z., Singh, V.P., Lin, Q., Ning, S., Zhou, Y., Jin, J., Zhou, R., Ma, Q., 2023. Agricultural drought characteristics in a typical plain region considering irrigation, crop growth, and water demand impacts. Agric. Water Manag. 282, 108266. https://doi.org/10.1016/j.agwat.2023.108266.
Zhao, G., Bates, P., Neal, J., 2020. The impact of dams on design floods in the conterminous US. Water Resour. Res. 56 (3) e2019WR025380.
Zhou, S.L., McMahon, T.A., Walton, A., Lewis, J., 2002. Forecasting operational demand for an urban water supply zone. J. Hydrol. 259 (1–4), 189–202. https://doi.org/10.1016/S0022-1694(01)00582-0.